Ir(I)-NHC Hybrid Materials: Surface-Stabilization of Low-Valent Iridium Species for High Catalytic Hydrogenation Performances

Iuliia Romanenko,[a] David Gajan,[b] Reine Sayah,[a] Delphine Crozet,[a] Erwan Jeanneau,[c] Christine Lucas,[a] Lénaic Leroux,[b] Laurent Veyre,[a] Anne Lesage,[b] Lyndon Emsley,[b],[d] Emmanuel Lacôte,[a],* Chloé Thieuleux[a],*

Abstract: An Ir(I)-NHC based hybrid material was prepared using a synthetic methodology allowing the precise positioning and isolation of the Ir-centers along the pore-channels of a silica framework. The full characterization of the material by solid state NMR spectroscopy showed that the supported Ir-sites were stabilized by the silica surface as low-coordinated single-site complexes. The material was found to be extremely efficient for the hydrogenation of functional alkenes. The catalytic performances (TOF and TON) are one to two orders of magnitude higher than those of their molecular Ir-analogues, which could be related to the prevention of bi-molecular deactivation processes of Ir-complexes observable under homogeneous conditions

Catalytic hydrogenation is one of the most important reactions for both bulk and fine chemical production.[1] As a consequence, the quest for ever more active and selective catalytic systems is essential. Late transition metal complexes stand out among the numerous options because their coordination sphere can be fine tuned for better efficiency, selectivity and stereoselectivity. That is especially true for iridium, one of the most active metals for catalytic hydrogenations.[2] However, in solution iridium complexes tend to rapidly form inactive polymetallic hydride clusters via bimolecular processes, leading to deactivation.[3]

One strategy to prevent this deactivation path is to slow down the oligomerization of the iridium hydrides in solution by modifying the coordination sphere of the iridium[4a] or using weakly coordinating anions (for cationic Ir(I) catalysts).[4b,c] Another option is to graft or intercalate the Ir(I) sites on a solid support, to physically prevent them from assembling into inactive clusters.[5] The latter is appealing because heterogeneous catalysts are easier to remove from products. However, the "heterogeneized" catalysts prepared by grafting or intercalation approaches usually exhibit low to similar activity in comparison with their homogeneous equivalents.[5a-d] We hypothesized that this decrease of activity was due to a lack of control of the metal distribution on the solid supports, and that hybrid materials containing strongly coordinated and precisely positioned supported Ir(I)-sites would be much more efficient hydrogenation catalysts.

In this respect, we proposed a general strategy for the preparation of late transition metal-based catalytic materials which relies on a two-step approach.[6] The first step is the preparation of hybrid mesostructured silica matrices containing regularly distributed L-type ligands by a sol-gel process using a templating route.[7] The L-ligand of the platform material is then *in-situ* converted into the targeted supported organometallic complex by Surface Organometallic Chemistry (SOMC).[8]

The hybrid silica material is prepared by co-hydrolysis and co-condensation of an organotrialkoxysilane precursor and a tetra-alkoxysilane in the presence of a structure directing agent in order to control the loading and organic groups homogeneity along the silica pore-channels. This control is mandatory to ensure that the catalytically active sites in the final material are well isolated from each other.

Using this methodology, we have investigated the immobilization on silica matrices of reactive Pd^{II},[6c] Ru^{IV}[6d-e] and Ir^{III}[6b] species as their N-heterocyclic carbene (NHC) complexes. The resulting materials are as active as their molecular equivalents.

Here, we coordinate Ir(I) centers to a silica-supported NHC ligand, because the Ir-NHC bond is strong[9]and NHCs also offer a good alternative to phosphine ligands classically used in iridium-catalyzed hydrogenation. [2a] A flexible propyl tether was chosen to allow Ir/silica interactions. Such a metal/support interaction was found to be the key for increasing the lifetime of Ru-NHC active species by stabilizing low-valent species[6e] and we felt that it might be extended to stripped-down Ir-NHC complexes, leading to even more active catalysts (see **M-Ir** on Scheme 1).

The preparation of the materials relies on the incorporation of iridium onto our previously described NHC-based material **M-Im** (Scheme 1).[6b]

[a] I. Romanenko, Dr. R. Sayah, Dr. D. Crozet, C. Lucas, L. Veyre, Dr. E. Lacôte, Dr. C. Thieuleux
Université de Lyon, Institut de Chimie de Lyon, UMR C2P2 CNRS, Université Lyon 1-ESCPE Lyon
43 Bd du 11 Novembre 1918, 69616 Villeurbanne (France)
E-mail: emmanuel.lacote@univ-lyon1.fr, chloe.thieuleux@univ-lyon1.fr

[b] Dr. D. Gajan, L. Leroux, Dr. A. Lesage, Prof. L. Emsley
Université de Lyon, Institut des Sciences Analytiques, CRMN CNRS-ENS Lyon-UCBL
5 rue de la Doua, 69100 Villeurbanne (France)

[c] Dr. E. Jeanneau
Université Lyon 1, Centre de Diffractométrie H. Longchambon
Site CLEA – Bât. ISA
5 rue de la Doua, 69100 Villeurbanne (France)

[d] Prof. L. Emsley
Institut des Sciences et Ingénierie Chimiques, Ecole Polytechnique Fédérale de Lausanne (EPFL), 1015 Lausanne (Switzerland)

Supporting information for this article is given via a link at the end of the document

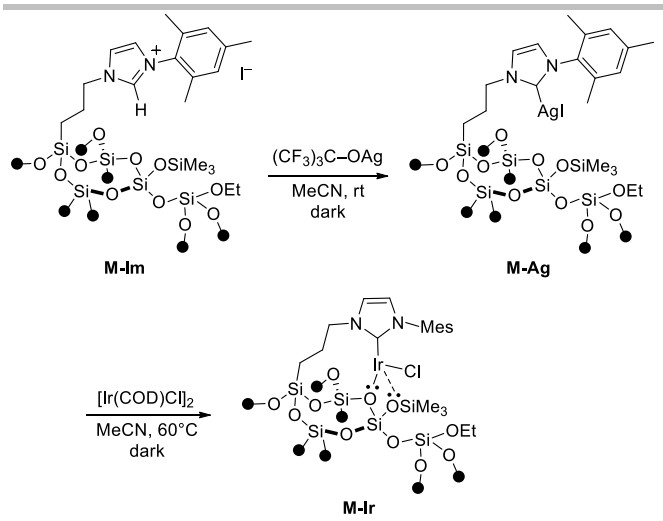

Scheme 1. Scheme for the preparation of the hybrid catalyst **M-Ir**

Passivated platform material **M-Im** (390 m^2/g surface area) was first metallated to the silver-carbene containing material **M-Ag** with 1.5 equivalents of $AgOC(CF_3)_3$ in MeCN at 25 °C in the absence of light. Transmetalation with 7 equiv. of $[IrCl(COD)]_2$ at 60 °C in MeCN delivered **M-Ir** as a brown powder containing 2.57 wt% Ir (0.13 mmol/g) corresponding to 49% silver to iridium conversion. **M-Ir** was characterized by XRD (Fig. S1), TEM (Fig. S2), and conventional ^{13}C, ^{29}Si MAS-NMR (Fig. S3-4) as well as DNP SENS (*vide infra*). We also prepared the ^{13}C-labeled material **M*-Ir** from the corresponding **M-Im***, where the carbene carbon was isotopically enriched. Finally, the complex [IrCl(COD)(MesImPr)] **1** was synthesized *via* a known route[10] and characterized by HRMS, ^1H, ^{13}C and ^1H-^{13}C HMQC NMR (Fig. S5). The XRD structure of **1** was also elucidated (Fig. S6).[11] This complex was prepared as a molecular standard for both materials characterization and for sake of comparison in the catalytic study.

The most important feature in **1** is that the iridium complex loses symmetry upon transmetallation because of its square planar structure and the dissymmetry of the NHC ligand. Thus, all carbons of the 1,5-cyclooctadiene ligand (COD) are inequivalent. The methylene ^{13}C signals in C_6D_6 appear at 29.4, 29.1, 33.3 and 34.9 ppm, while the sp^2 carbons are at 50.3, 51.1 (*trans* to Cl) and 83.1 and 83.2 (*trans* to NHC).

^{29}Si CPMAS NMR of **M-Ir** shows the presence of the expected four main peaks: 13 (M), –65 (T_3), –100 (Q_3), –109 ppm (Q_4) (Fig. S3). The first peak corresponds to the $SiMe_3$ surface groups and shows that passivation was successful, while the presence of a T_3 peak shows that the organosilane residue is completely fused within the silica network leading to a fully condensed tetrahedral Si surface site. In the ^{13}C CPMAS NMR spectrum (Fig. S4), the expected signals arising from the propyl tether and the NHC ligand were observed around 9 ppm (Si–**C**H_2), 18-20 ppm (methyl groups of the mesityl substituent and Si–CH_2–**C**H_2), 52 ppm (**C**H_2–N) and 120-140 ppm (aryl and NHC sp^2 carbons). Interestingly, the ^{13}C peaks corresponding to the COD ligand were not detected (*vide infra*).

TEM micrographs and EDX analyses showed the presence of silver aggregates arising from production of the silver halide salt during the transmetallation process. TEM micrographs do not indicate the presence of any Ir nanoparticle, while EDX performed on several zones of the material provided similar Ir loadings, suggesting a homogeneous distribution of the Ir throughout all the material (see Figure S7). These observations suggest that iridium is present as a supported coordination complex, not as metal nanoparticles.

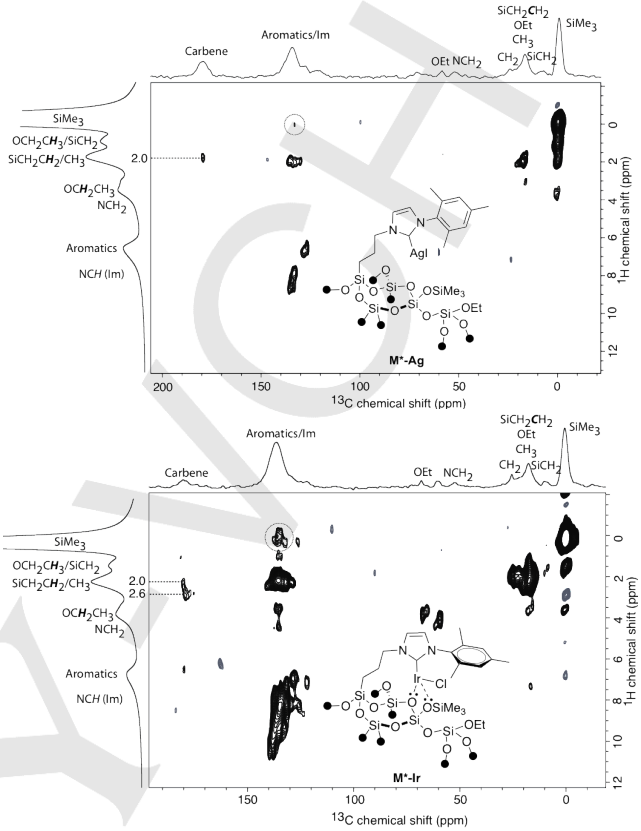

Figure 1. 2D ^1H-^{13}C HETCOR NMR spectra of **M*-Ag** and **M*-Ir** recorded on a 800 MHz with a long contact time (2 ms). The top traces are the corresponding 1D ^{13}C CPMAS spectra and the left traces the corresponding 1D ^1H Hahn echo spectra. (See SI for experimental details).

To shed light on the nature of the iridium species, and their possible interaction with the silica surface, we compared the 2D HETCOR NMR spectra of the labeled materials **M*-Im**, **M*-Ag** and **M*-Ir** at long (Figure 1 and S10) and short (Fig. S11) contact times to discriminate directly bonded ^1H and ^{13}C vs. spatially close ^1H and ^{13}C atoms. At a long contact time, correlation spots were found between the protons of the surface trimethylsilyl (TMS) groups and the aromatic carbons of the mesityl for all materials, suggesting that the NHC is folded toward the surface. More interestingly, the sole crosspeak assigned to the carbene in the ^1H-^{13}C HETCOR of **M*-Ag** (Fig. 1, top) is split after Ir transmetallation (Fig. 1, bottom). This is attributed to the formation of the Ir-NHC along with residual Ag-NHC species. This observation is consistent with a splitting of the NMR signal of the same methyl groups in **1**. Here again, no signal attributed to COD was detected, strongly suggesting its absence in the Ir coordination sphere. Taking into account that the NHC folds toward the surface, one may hypothesize that the Ir sites are stabilized by surface Si–O–Si groups after decoordination of 1,5-cyclooctadiene. In order to discard any possible uncertainty due to the limited sensitivity of conventional MAS NMR, we implemented advanced dynamic nuclear polarization surface enhanced NMR spectroscopy (DNP SENS)

experiments.[12] The samples were prepared by impregnation of the materials with a solution of 16 mM TEKPOL in 1,1,2,2-tetrachloroethane and the spectra were recorded on a 400 MHz/263 GHz gyrotron DNP NMR system. In this setup, EPR transitions of the radical are saturated at 100 K by microwaves which induces transfer of the electron spin polarization to nuclei of interest at the silica surface, resulting in large NMR signal enhancement.

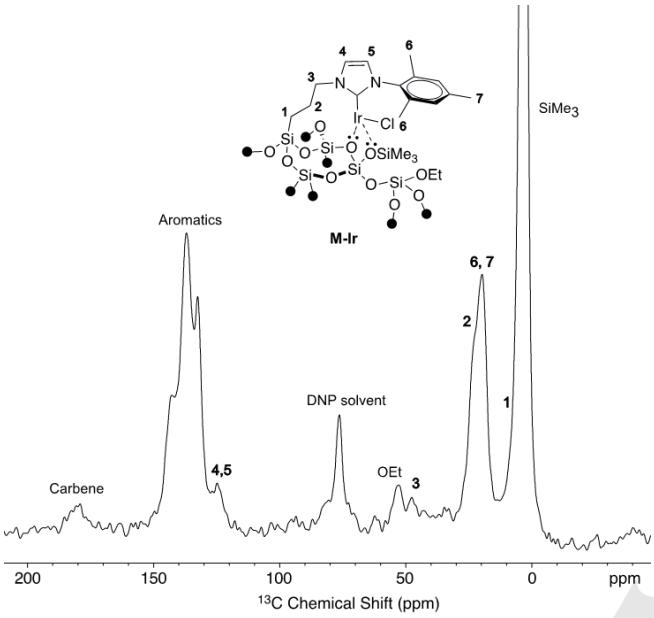

Figure 2. ^{13}C CP MAS solid echo DNP SENS spectrum of **M-Ir** recorded on a 400MHz DNP NMR system with an echo time of 40 rotor periods (see SI for details).

Again, no signal in the COD region was detected in the ^{13}C DNP SENS experiments (Fig. 2 and S12). Similarly, no correlation signal involving a COD was observed in 2D DNP SENS ^{1}H-^{13}C HETCOR spectra (Fig S13). However, 2D DNP SENS ^{1}H-^{29}Si HETCOR (Fig. S14a) showed a correlation between Q signals at –100 ppm and the NHC backbone and mesityl protons even with short contact times. At longer contact times (Fig. S14b), crosspeaks between the $SiMe_3$ and the aromatics appeared in addition. As this method assesses the spatial proximity of protons to the silicon centers,[12b] this further suggests that the spacer folds toward the surface to stabilize a COD-free Ir species.

We finally attempted to prove the absence/presence of COD by a chemical method. We exposed a C_6D_6 suspension containing **M-Ir** and toluene as an internal standard to hydrogen in a pressure-stable NMR tube without an olefinic substrate, and monitored the reaction by solution ^{1}H NMR. We were able to detect trace amount of cyclooctane, whose quantification against toluene (Figure S15–S16) revealed that only 8 % of Ir sites contain COD.[13]

To conclude, we have shown that surface-metal interactions stabilize a supported low-coordinated iridium complex, whose structure we tentatively assign in Figure 1. *This has to our knowledge never been observed before in Ir-chemistry*. A similar phenomenon between supported Ru complexes and the surface was already suggested, but not directly observed for the surface metal complex.[6e]

The catalytic activity of the **M-Ir** material was tested in the hydrogenation of several functional substrates (styrenes with various substituents, stilbene and limonene (TableS4)). In a typical catalytic experiment, a solution of *trans*-stilbene in toluene was heated at 40°C in a Fisher-Porter reactor under 3 bar of dihydrogen in the presence of 0.1 mol% **M-Ir** (based on iridium loading given by elemental analysis). The reaction was followed by solution NMR to build its conversion *vs*. time profile (Figure 3). Full conversion was observed after 18 h. The same reaction using **1** under homogeneous conditions failed to reach full conversion after more than 80 days! Cationic iridium species $[Ir(COD)(MesImPr)]BF_4$ *in-situ* generated from $[IrCl(COD)(MesImPr)]$ with $AgBF_4$ under homogeneous conditions worked faster, but even then the reaction was not over after 60 days. Moreover, a blank test using the parent material **M-Ag** left the substrate unchanged, showing that catalysis was due to the Ir centers in the material.

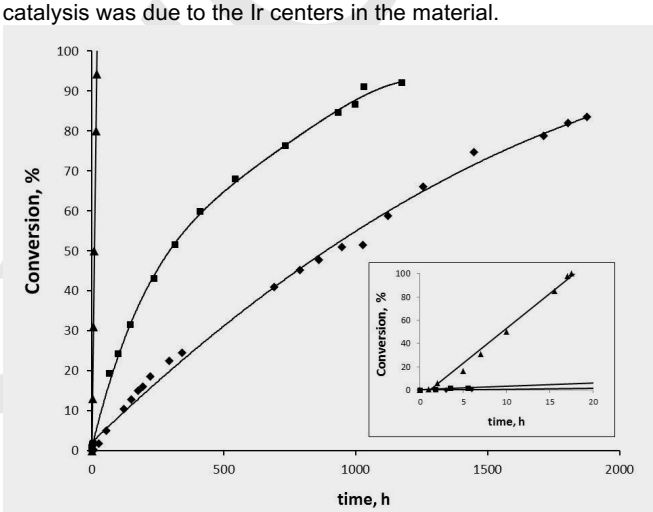

Figure 3. Conversion of *trans*-stilbene hydrogenation as a function of reaction time using: the neutral organometallic complex **1** (♦diamonds); cationic $[Ir(COD)(MesImPr)]BF_4$ (■ squares); **M-Ir** material (▲triangles). The hydrogenation experiments were carried out in toluene at 40 °C under 3 bar of H_2 (0.1 mol% of Ir).

We calculated the initial TOFs (after 5h of reaction) for **M-Ir**, the neutral complex **1** and its cationic form: TOF= $38h^{-1}$ for **M-Ir** vs $1.8h^{-1}$ for $[Ir(COD)(MesImPr)]BF_4$, and $0.75h^{-1}$ for **1**. The material is thus 50 times faster than **1**, and 20 times faster than $[Ir(COD)(MesImPr)]BF_4$, fully validating our hypotheses. Furthermore, the hydrogenation profile of **M-Ir** in Fig. 3 is linear thus suggesting no catalyst deactivation of the catalysts during the catalytic test.

We evaluated the heterogeneous catalyst activity using very high substrate/catalyst ratios (0.01 mol%, Figure 4). While both homogeneous complexes are deactivated and only reach a $TON_{max} \leq 1000$ after 700 h (observation of the catalyst deactivation at 89% conversion using 0.1 mol% of **1**), **M-Ir** exhibited a much higher productivity reaching 80% conversion (TON = 8000 using 0.01mol% of **M-Ir**)). After catalysis the solid was analyzed by HRTEM. We did not see any trace of Ir nanoparticles in the recovered catalyst. Unfortunately, we could not determine the TON_{max}. The trace impurities remaining after purification of the large amounts of solvent and substrate needed for the tests induced side poisoning of the 60mg of catalyst needed for reproducibility at the high substrate/Ir ratios required for TON_{max} determination.

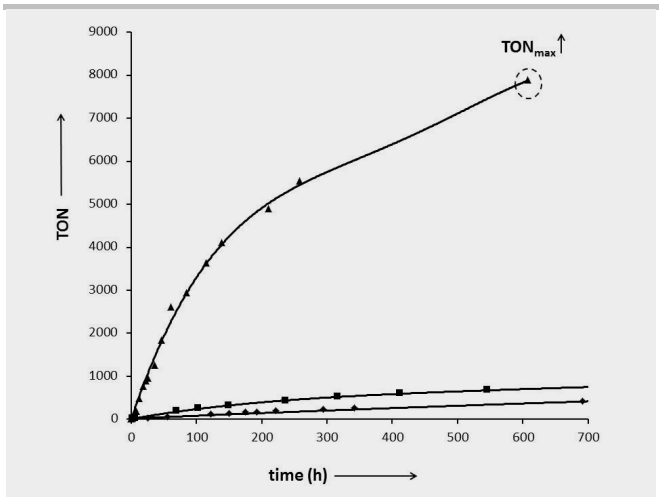

Figure 4. TON of *trans*-stilbene hydrogenation as a function of reaction time using: **1** (♦diamonds); [Ir(COD)(MesImPr)]BF_4 (■ squares); **M-Ir** (▲triangles). The hydrogenation experiments were carried out in toluene at 40°C under 3 bar of H_2 (0.1 mol% of Ir for 1 and [Ir(COD)(MesImPr)]BF4; 0.01mol% of Ir for M-Ir)

Split tests were carried out using **M-Ir** (Fig S19). No conversion was detected, thus showing the absence of any active Ir-species in solution. Finally, no leaching of Ir was detected in the reaction supernatants by ICP measurements. Therefore, there is no contribution of any homogeneous pathway. The catalytic hydrogenation takes place on Iridium surface sites of the material.

The behavior of the other substrates (styrene, 4-fluorostyrene, 4-vinylanisole, 4-acetoxystyrene and limonene) is shown in the supporting information. In all cases, the material is better than **1** (Figure S18 and part 7). For limonene, the less hindered bond is fully hydrogenated before the more substituted one started reacting.

In summary, we have prepared a well-defined single-site Ir(I)-NHC based heterogeneous catalyst in which the iridium atoms are homogeneously positioned by design. Using advanced solid state NMR techniques, and a chemical method we showed that the Ir centers are stabilized by the surface as low-coordinated complexes. This catalytic material is one to two orders of magnitude more active and faster than its molecular analogue in the hydrogenation of *trans*-stilbene, and also faster than the corresponding cationic species. This enhanced activity was also observed for other functional olefins. It derives from the isolation of the supported Ir-NHC species, which prevents the bimolecular deactivation processes (hydride cluster formation) usually encountered for Ir complexes in solution. Interactions between the silica surface and the Ir sites, which stabilize a low-valent Ir(I) species were evidenced for the first time in Ir catalysis. They likely also account for the higher catalytic performances of **M-Ir**.[13]

The strategy whereby more active catalysts are obtained by preventing deactivation of bimolecular processes and using the support to stabilize more reactive species is of interest for many other catalytic systems. Further work will focus on extending this approach towards the preparation of highly selective heterogeneous Ir asymmetric catalysts.

Acknowledgements

We thank CNRS, CPE, Université Claude Bernard Lyon 1, ANR (CFLOW-OM, NHCX) and Total (postdoctoral funding to D. C.) for financial support of this work. I. R. thanks CNRS/CPE for a doctoral stipend. TGIR RMN THC (FR 3050 CNRS) and ERC Advanced grant number 320860, are kindly acknowledged for the NMR characterizations. We thank CTμ for the TEM measurements.

Keywords: Hydrogenation • Heterogeneous catalysis • Mesoporous materials • Iridium • Carbene ligands

[1] a) The Handbook of Hydrogenation (Eds: J.G. de Vries, C.J. Elsevier), WILEY-VCH Verlag GmbH & Co, **2007**. b) W. S. Knowles *Angew. Chem. Int. Ed*. **2002**, 41(12), 1998-2007; c) W. Bonrath, J. Medlock, J. Shütz, B. Wüstenberg, T. Netscher in Hydrogenation (Eds.: I. Karame), InTech, **2012**, pp. 69-90.

[2] a) Iridium complexes in organic synthesis (Eds: L. Oro, C. Claver), WILEY-VCH Verlag GmbH & Co, **2008.** b) *Iridium Catalysis, Topics in Organometallic Chemistry Vol. 34* (Ed.: P.G. Andersson), Spriger-Verlag Berlin Heidelberg, **2011**, pp. 1-76; c) R. Crabtree, *Acc. Chem. Res*. **1979**, *12*, 331-337

[3] a) Y. Xu, M. A. Celik, A. L. Thompson, H. Cai, M. Yurtsever, B. Odell, J. C. Green, D. M. P. Mingos, J. M. Brown, *Angew. Chem. Int. Ed.* **2009**, *48*, 582-593; b) S. P. Smidt, A. Pfaltz, E. Martínez-Viviente, P. S. Pregosin, A. Albinati, *Organometallics* **2003**, *22*, 1000-1009; c) X. Cui, Y. Fan, M. B. Hall, K. Burgess, *Chem. Eur. J*. **2005**, *11*, 6859-6868; d) L. D. Vazquez-Serrano, B. T. Owens, J. M. Buriak, *Chem. Commun*. **2002**, 2518-2519; e) J. Campos, L. S. Sharninghausen, R. H. Crabtree, D. Balcells, *Angew. Chem. Int. Ed.* **2014**, *53*, 12808-12811; f) Homogeneous Catalysts: Activity – Stability – Deactivation, First Edition (Eds: P.W.N.M. van Leeuwen, J.C. Chadwick), Wiley- VCH Verlag GmbH & Co, **2011**

[4] a) Y. Xu, D. M. P. Mingos, J. M. Brown, *Chem. Commun*. **2008**, *2*, 199-201; b) S. P. Smidt, N. Zimmermann, M. Studer, A. Pfaltz, *Chem. Eur. J*. **2004**, *10*, 4685-4693; c) S. Gruber, M. Neuburger, A. Pfaltz, *Organometallics* **2013**, *32*, 4702-4711; d) L. D. Vazquez-Serrano, B. T. Owens, J. M. Buriak, *Inorg. Chim. Acta* **2006**, *359*, 2786-2797.

[5] For Ir catalysts heterogeneized on silica supports, see: a) B. Pugin, H. Landert, F. Spindler, H.-U. Blaser, *Adv. Synth. Catal.* **2002**, *344*, 974-979; b) C. González-Arellano, A. Corma, M. Iglesias, F. Sánchez, *Inorganica Chim. Acta* **2004**, *357*, 3071-3078; c) S. Sahoo, P. Kumar, F. Lefebvre, S. B. Halligudi, *J. Catal.* **2008***, 254,* 91-100. ; for other types of supports d) M. Crocker, R.H.M. Herold, *Cat.Let.***1993, *18,*** 243-251; e) M. Blanco, P. Álvarez, C. Blanco, M. Vi. Jiménez, J. Fernández-Tornos, J. J. Pérez-Torrente, L. A. Oro, R. Menéndez, *ACS Catal.* **2013**, *3*, 1307-1317.

[6] a) M. P. Conley, C. Copéret, C. Thieuleux, ACS Catal. **2014**, *4*,1458-1469; b) T. K. Maishal, J. Alauzun, J.-M. Basset, C. Copéret, R. J. P. Corriu, E. Jeanneau, A. Mehdi, C. Reyé, L. Veyre, C. Thieuleux, *Angew. Chem. Int. Ed.* **2008**, *47*, 8654-8656; c) M. P. Conley, R. M. Drost, M. Baffert, D. Gajan, C. Elsevier, W. T. Franks, H. Oschkinat, L. Veyre, A. Zagdoun, A. Rossini, M. Lelli, A. Lesage, G. Casano, O. Ouari, P. Tordo, L. Emsley, C. Copéret, C. Thieuleux, *Chem. Eur. J.* **2013**, *19*, 12234-12238; d) I. Karamé, M. Boualleg, J.-M. Camus, T. K. Maishal, J. Alauzun, J.-M. Basset, C. Copéret, R. J. P. Corriu, E. Jeanneau, A. Mehdi, C. Reyé, L. Veyre, C. Thieuleux, *Chem. Eur. J.* **2009**, *15*, 11820-11823; e) M. K. Samantaray, J. Alauzun, D. Gajan, S. Kavitake, A. Mehdi, L. Veyre, M. Lelli, A. Lesage, L. Emsley, C. Copéret, C. Thieuleux, *J. Am. Chem. Soc.* **2013**, *135*, 3193-3199.

[7] a) S. L. Burkett, S. D. Sims, S. Mann, *Chem. Commun*. **1996**, 1367-1368; b) D. J. Macquarrie, *Chem. Commun*. **1996**, 1961-1962; c) D. Margolese, J. A. Melero, S. C. Christiansen, B. F. Chmelka, and G. D. Stucky, *Chem. Mater*. **2000**, *12*, 2448-2459; d) L. Mercier, T. J. Pinnavaia, *Chem. Mater*. **2000**, *12*, 188-196; For a review, see: e) F. Hoffmann, M. Cornelius, J. Morell, M. Fröba, *Angew. Chem. Int. Ed.* **2006**, *45*, 3216-3251.

[8] C. Copéret, M. Chabanas, R. Petroff Saint-Arroman, J.-M. Basset, *Angew. Chem. Int. Ed.* **2003**, *42*, 156-181.

[9] a) H. M. Lee, T. Jiang, E. D. Stevens, S. P. Nolan, *Organometallics* **2001**, *20*, 1255-1258; b) M. T. Powell, D.-R. Hou, M. C. Perry, X. Cui, K. Burgess, *J. Am. Chem. Soc.* **2001**, *123*, 8878-8879; c)Y. Zhu, Y.Fan, K. Burgess, *J.Am.Chem. Soc.* **2010**, *132*, 6249-6253; d) I. Kownacki, M. Kubicki, K. Szubert, B. Marciniec, J. Organomet. Chem. 2008, *693*, 321-328; e) G. E. Dobereiner, A. Nova, N. D. Schley, N. Hazari, S. J. Miller, O. Eisenstein, R. H. Crabtree, *J. Am. Chem. Soc.* **2011**, *133*, 7547-7562; f) L. S. Bennie, C.J. Fraser, S. Irvine, W.J. Kerr, S. Andersson, G. Nilsson, *Chem. Commun.* **2011**, 11653-11655; g) N-Heterocyclic Carbenes: Effective Tools for Organometallic Synthesis, First Edition (Eds: S. P. Nolan), Wiley VCH Verlag GmbH & Co, **2014**.

[10] H. M. J. Wang and I.J. B. Lin, Organometallics 1998, *17*, 972-975

[11] The crystallographic data have been deposited at the CCDC [ref. CCDC 1043116]

[12] a) A. Lesage, M. Lelli, D. Gajan, M. A. Caporini, V. Vitzthum, P. Miéville, J. Alauzun, A. Roussey, C. Thieuleux, A. Mehdi, G. Bodenhausen, C. Copéret, L. Emsley *J. Am. Chem. Soc.* **2010**, *132*, 15459-15461; b) M. Lelli, D. Gajan, A. Lesage, M. A. Caporini, V. Vitzthum, P. Mieville, F. Heroguel, F. Rascon, A. Roussey, C. Thieuleux, M. Boualleg, L. Veyre, G. Bodenhausen, C. Coperet, L. Emsley, *J. Am. Chem. Soc.* **2011**, *133*, 2104-2107. For a review, see: c) A. Rossini, A. Zagdoun, M. Lelli, A. Lesage, C. Copéret, L. Emsley *Acc. Chem. Res.* **2013**, *46*, 1942-1951.

[13] Beside the evolution of COD, the hydrogenation of C_6D_6 was observed, as shown by the growth of a broad signal at ca. 1.37 ppm, corresponding to deuterated cyclohexane. This result and the slight color modification suggest the formation of Ir nanoparticles in that case. For a reference on benzene room temperature hydrogenation with Ir nanoparticles, see: E. Bayram, M. Zahmakiran, S. Özkar, R. G. Finke, *Langmuir* **2010**, *26*, 12455-12464. The presence of Ir NPs in the spent catalysts was further confirmed by TEM and EDX analyses (See Fig. S17 in SI)

[13] Rimoldi, A. Mezzetti, *Inorg. Chem.* **2014,** *53*, 11974-11984.

Entry for the Table of Contents (Please choose one layout)

Layout 2:

COMMUNICATION

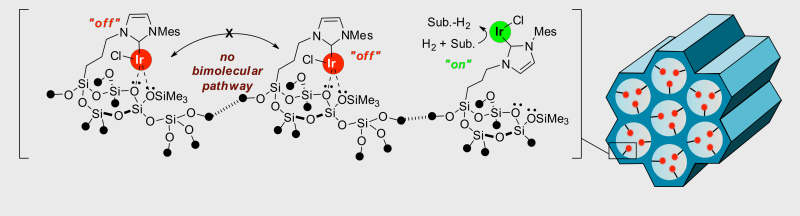

Homogeneous positioning of Ir(I) complexes in the pore-channels of a silica framework stabilizes a low-valent Ir(I) species and lead to drastic improved catalyst efficiency. Catalyst decomposition by formation of iridium-hydride clusters is prevented by the attachment on the support.

Iuliia Romanenko, David Gajan, Reine Sayah, Delphine Crozet, Erwan Jeanneau, Lénaic Leroux, Christine Lucas, Laurent Veyre, Anne Lesage, Lyndon Emsley, Emmanuel Lacôte, Chloé Thieuleux**

Page No. – Page No.

Ir(I)-NHC Hybrid Materials: Surface-Stabilization of Low-Valent Iridium Species for High Catalytic Hydrogenation Performances

Supporting information

Ir(I)-NHC Hybrid Materials: Surface-Stabilization of Low-Valent Iridium Species for High Catalytic Hydrogenation Performances

Iuliia Romanenko,[a] David Gajan,[b] Reine Sayah,[a] Delphine Crozet,[a] Erwan Jeanneau,[c] Christine Lucas,[a] Lénaic Leroux,[b] Laurent Veyre,[a] Anne Lesage,[b] Lyndon Emsley,[b],[d] Emmanuel Lacôte,[a],* Chloé Thieuleux[a],*

[a] Université de Lyon, Institut de Chimie de Lyon, LC2P2, UMR 5265 CNRS-CPE Lyon-UCBL, CPE Lyon43, Bd du 11 Novembre 1918,69616 Villeurbanne, France.

[b] Centre de RMN à Très Hauts Champs, Institut de Sciences Analytiques (CNRS / ENS Lyon / UCB Lyon 1), Université de Lyon, 69100 Villeurbanne, France.

[c] Centre de Diffractométrie H. Longchambon Site CLEA – Bât. ISA, 5 rue de La Doua 69100 Villeurbanne, France.

[d] Institut des Sciences et Ingénierie Chimiques, Ecole Polytechnique Fédérale de Lausanne (EPFL), 1015 Lausanne (Switzerland)

Table of contents

1. General information

All the reactions related to surface-modifications and synthesis of [IrCl(COD)(MesImPr)] were carried out under Ar using standard Schlenk technics and dry degassed solvents. Mesitylimidazole and $AgOC(CF_3)_3$ were synthesized in our laboratory according to the literature procedure.[1] TEOS (tetraethylorthosilicate), HI, Ag_2O, Pluronic123, TMSBr were bought from Sigma-Aldrich. TEOS was distilled over Mg before use. The metal complex $[IrCl(COD)]_2$ was received from Strem Chemicals and used without further purification.

Elemental analyses were performed under inert atmosphere at the Mikroanalytisches Labor Pascher, Remagen, Germany.

Liquid state NMR spectra were recorded using a Bruker AC 300MHz (for catalysis) and 400MHz (for NMR experiments under H_2 pressure). MAS NMR spectra were recorded on a Bruker Advance 300 MHz spectrometer (for ^{29}Si NMR) and 500 MHz spectrometer (for ^{1}H, ^{13}C NMR) with a conventional double resonance 4 mm CP-MAS probe. The MAS frequency was set to 10 kHz for all the ^{1}H and ^{13}C experiments reported here and 5 kHz for ^{29}Si NMR. The analysis performed with a 4 mm probe.

2. Synthesis and characterization of Iridium(I) based NHC material

Synthesis of Material M-Ir. 2.6 g of protected material prepared as previously described,[1] was mixed with 0.782 g of $AgOC(CF_3)_3$ in glove box in the absence of light and dissolved in 45 ml of dried and degased CH_3CN. The mixture was left for stirring overnight at 25 °C. The solid was filtered under Ar and washed 3 times by degased and dried CH_3CN (20 ml) and CH_2Cl_2 (20 ml). The material was dried at 25 °C under the vacuum overnight. A brownish powder (2.5 g), **M-Ag**, was obtained and stored in glove box. Elemental Analysis: 0.72 % N; 4.27 % Ag; 36.8 % Si.

500 mg (0.17 mmol) of dried silver material, **M-Ag**, was mixed with 420 mg (1.25mmol) of $[IrCl(COD)]_2$ in glove box. Mixture was dissolved in 20 ml of dried and degased CH_3CN and left for stirring for 48 h at 60 ^oC. The powder was filtered under Ar and washed with dried and degased CH_3CN (20 ml) and CH_2Cl_2 (20 ml). Elemental Analysis: 0.79 % N; 33.7 % Si; 3.91 % Ag; 2.57 % Ir. The powder was characterized by TEM, X-ray diffraction and ^1H, ^{13}C and ^{29}Si NMR spectroscopy.

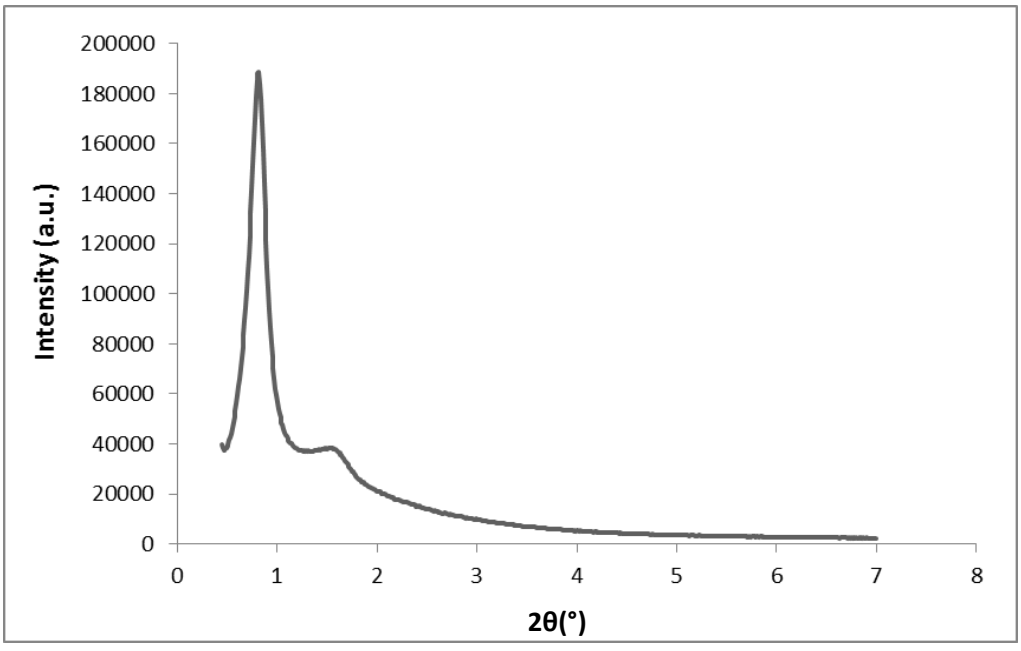

Figure S1. XRD pattern of **M-Ir**. The pattern exhibits an intense peak at 2θ = 0.82° (d =98 Å and a = 55 Å).

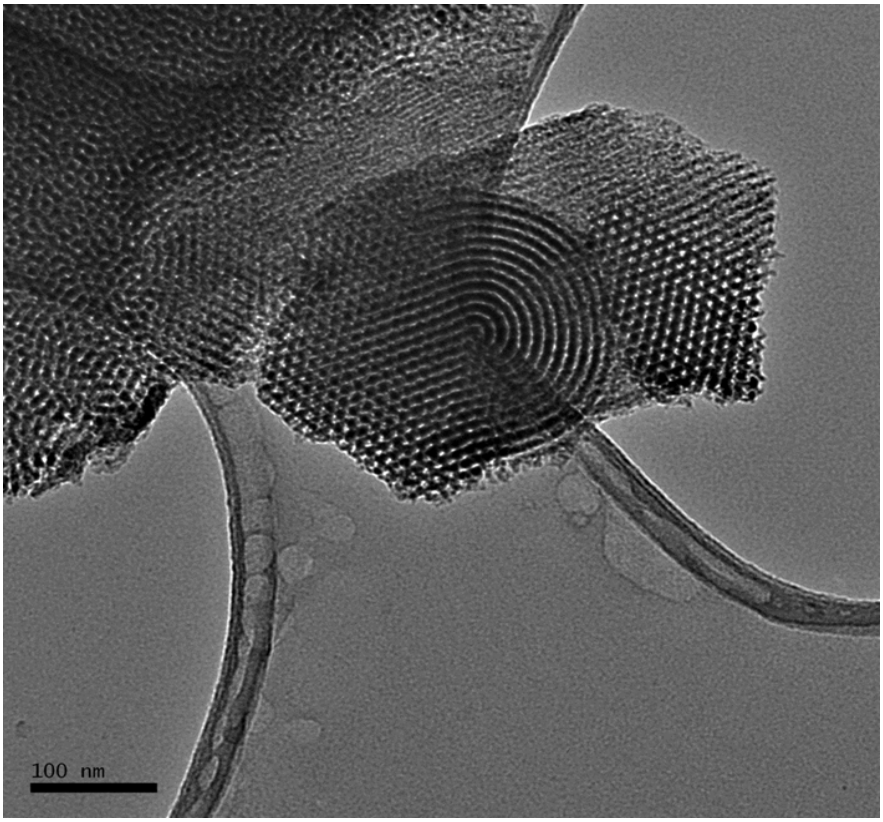

Figure S2. TEM micrograph of **M-Ir**. Material retains hexagonal symmetry after transmetallation.

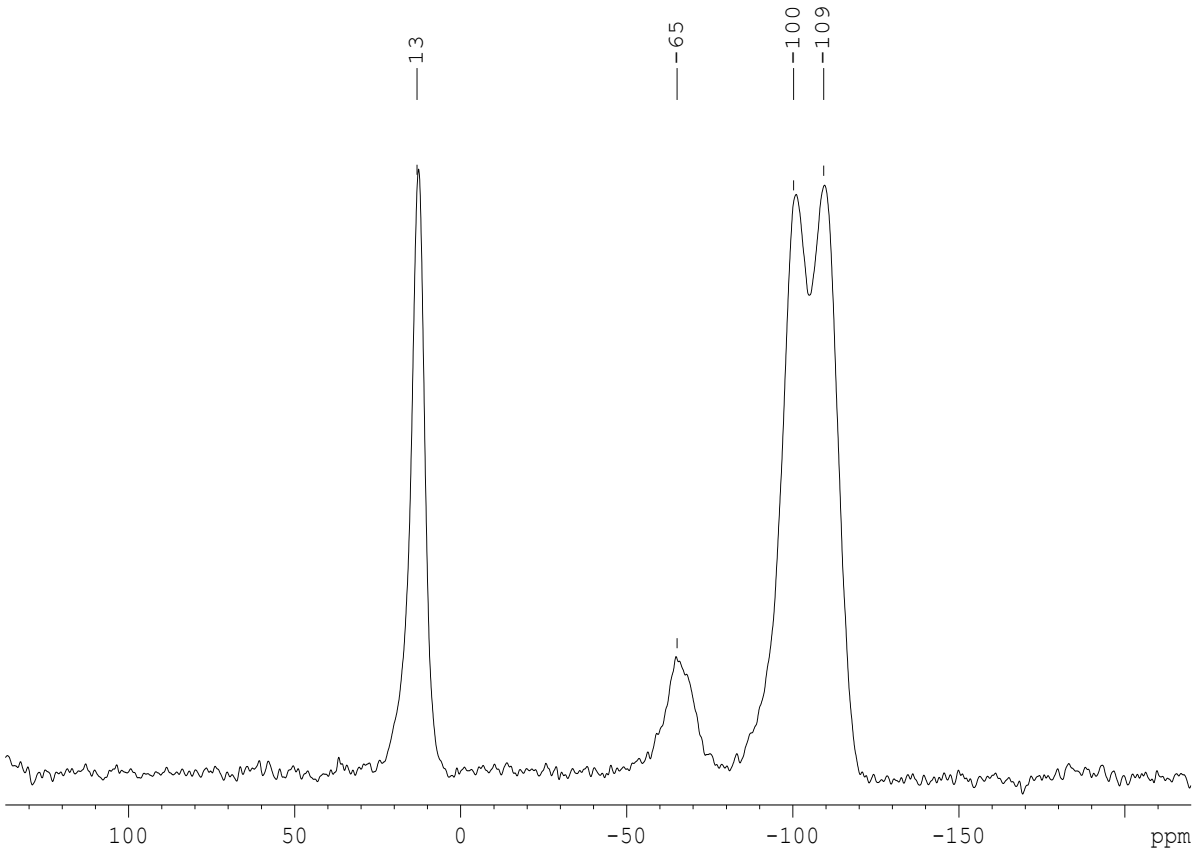

Figure S3. ^{29}Si CP-MAS NMR spectra **M-Ir** material. The peak at 13 ppm is attributed to surface TMS (Si-OTMS), at -65 ppm to T3 site (organic moieties perfectly incorporated in the silica matrix), and at -100 ppm and -109 ppm to Q3 and Q4 (silica matrix), respectively. To be more accurate, the peak at -100 ppm can be attributed to a Q4' corresponding to the passivation of Q3 site.. The spectrum was recorded at 300 MHz (proton frequency), with a spinning frequency of 5 kHz. A total of 30000 scans with recycle delay 2 seconds were accumulated.

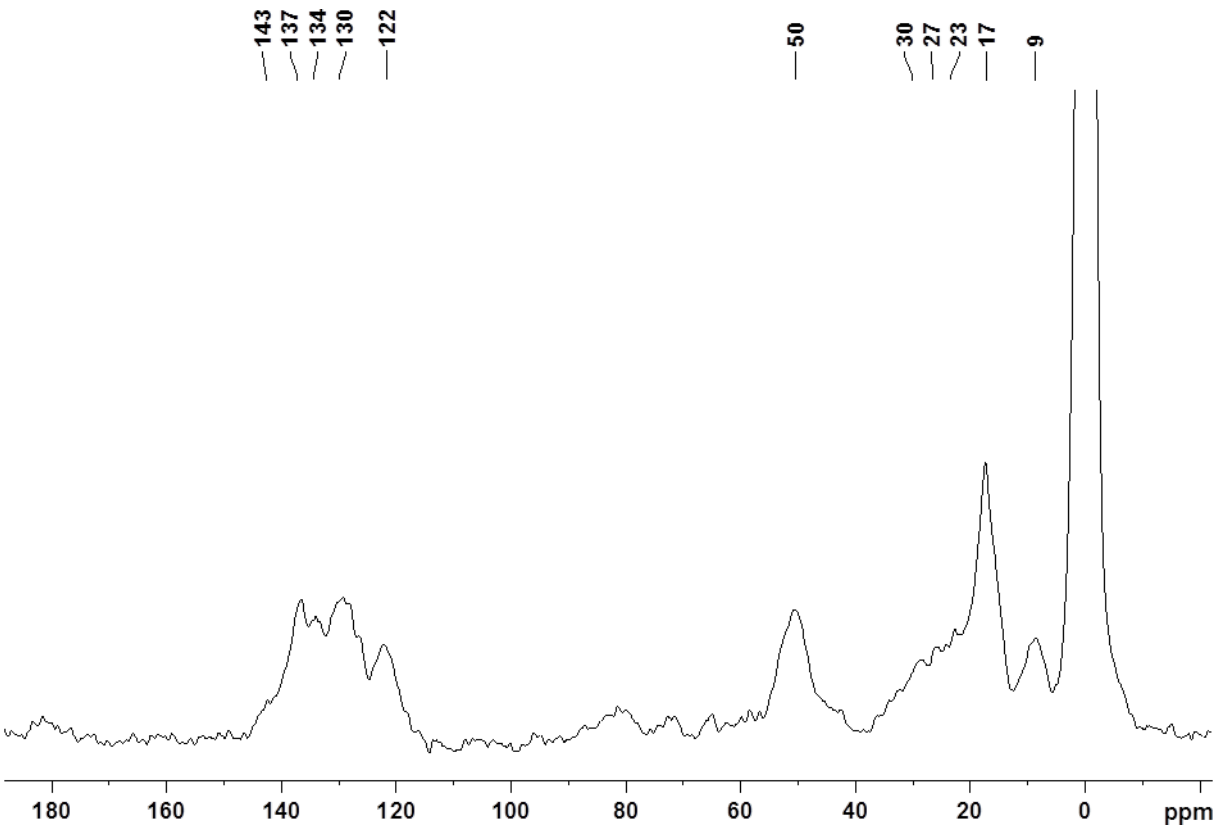

Figure S4. ^{13}C CP-MAS NMR spectrum of M-Ir material. Peaks at 120-140 ppm are attributed to aromatic carbons, 51 ppm for NCH_2, 20 ppm for CH_3 of mesityl and $SiCH_2\boldsymbol{C}H_2$, 10 ppm for $SiCH_2$ and 0 ppm for Si-OTMS. Signal at 61 ppm attributed to residual SiOEt groups. 184320 scans with a recycle delay 2 seconds were accumulated at 12.5 kHz.

3. Synthesis and characterization of [IrCl(COD)(MesImPr)] 1

200 mg (0.6 mmol) of dried MesImPrI were mixed with 67 mg (0.3 mmol) of Ag_2O in argon atmosphere in the absence of light. The mixture was dissolved in 20 ml of dried CH_3CN and left for stirring at 25 °C for 4 h. Then the rest of Ag_2O was filtered under inert conditions and transparent filtrate was evaporated under vacuum. The silver carbene was characterized by ^1H, ^{13}C NMR spectroscopy. 195 mg (0.3 mmol) of $[Ir(COD)Cl]_2$ were dissolved in 20 ml of dried and degased CH_3CN and transferred by cannula system to the silver carbene. The reaction was carried out at 60 ^oC during 12 h (time of reaction less than 5 h gives a mixture of products). The product was purified by column chromatography, using CH_2Cl_2 as eluent. The orange crystals of **1** were obtained by crystallization at -28 ^oC from CH_2Cl_2. The complex **1** was characterized by ^1H, ^{13}C, ^{13}C dept135 and 2D ^1H-^1H, ^1H-^{13}C NMR spectroscopy, ESI-MS and X-Ray diffraction.

^1H, ^{13}C NMR of [(MesImPr)AgI]

^1H NMR (C_6D_6, 300K): δ (ppm)= 0.62 (t, J=7.4 Hz, 3H, CH_3 of Pr); 1.36 (sext., J=7.1 Hz, 2H, $NCH_2\underline{CH_2}$ of Pr); 1.83 (s, 6H, CH_3 of Mes); 2.06 (s, 3H, CH_3 of Mes); 3.69 (t, J=6.9 Hz, 2H, NCH_2 of Pr); 5.90 (s, 1H, CH of Im); 6.09 (s, 1H, CH of Im); 6.65 (s, 2H, CH of Mes).

^{13}C NMR (C_6D_6, 300K): δ (ppm)=10.87 (CH_3 of Pr); 17.82 (*2*CH_3 of Mes); 20.99 (CH_3 of Mes); 24.59 ($NCH_2\underline{CH_2}$ of Pr); 52.84 (NCH_2 of Pr); 121.27(CH of Im); 120.31 (CH of Im); 129.34 (*2*CH of Mes); 134.92 (2C quat. of Mes); 136.17(C quat. of Mes), 138.67 (C quat. of Mes); 186.47 (C-Ag, Im).

^1H, ^{13}C NMR of [IrCl(COD)(MesImPr)] complex 1

^1H NMR (C_6D_6, 300K): δ (ppm)=0.78 (t, J=7.4 Hz, 3H, CH_3 of Pr); 1.25-1.45(m, 1H, CH_2 of COD), 1.50-1.65 (m, 5H, CH_2 of COD); 1.73 (s, 3H, CH_3 of Mes); 1,75-1.98 (m, 3H, CH_2 of COD); 1,98-2.09 (m, 1H, CH_2 of COD); 2.11 (s, 3H, CH_3 of Mes); 2.56 (s, 3H, CH_3 of Mes); 2.91 (ddd, J=13.0 Hz, J=8.1 Hz, J=7.1 Hz, 1H, =CH of COD); 3.14 (ddd, J=13.0 Hz, J=8.1 Hz, J=7.1 Hz, 1H, =CH of COD); 3.99 (td, J=7.1 Hz, J=2.5 Hz, 1H, NCH_2 of Pr); 4.80 (td, J=7.1 Hz, J=2.5 Hz, 1H, NCH_2 of Pr); 4.90-5.10 (m, 2H, =CH of COD); 5.91 (d, J=2.0Hz, 1H, CH of Im); 6.18 (d, 1H, CH of Im); 6.68 (s, 1H, CH of Mes); 6.77 (s, 1H, CH of Mes).

^{13}C NMR (C_6D_6, 300K): δ (ppm)=11.21 (CH_3 of Pr); 17.51 (CH_3 of Mes), 19.96 (CH_3 of Mes); 20.85 (CH_3 of Mes); 23.80 ($NCH_2\underline{CH_2}$, Pr); 29.33 (CH_2 of COD); 29.90 (CH_2 of COD); 33.44 (CH_2 of COD); 35.02 (CH_2 of COD); 50.95 (=CH of COD); 50.17 (=CH of COD); 53.12 (NCH_2 of Pr); 83.22 (*2*CH of COD); 122.37 (CH of Im), 120.60 (CH of Im); 129.84 (CH of Mes); 134.37(C quat. of Mes); 136.53(C quat. of Mes); 137.51(C quat. of Mes); 138.30 (C quat. of Mes); 180.60 (C-Ir, Im).

HRMS (ESI+): calculated for $[(MesImPr)Ir(Cod)(CH_3CN)]^+$ ([M-Cl + CH_3CN]) 570.2; found 570.2 .

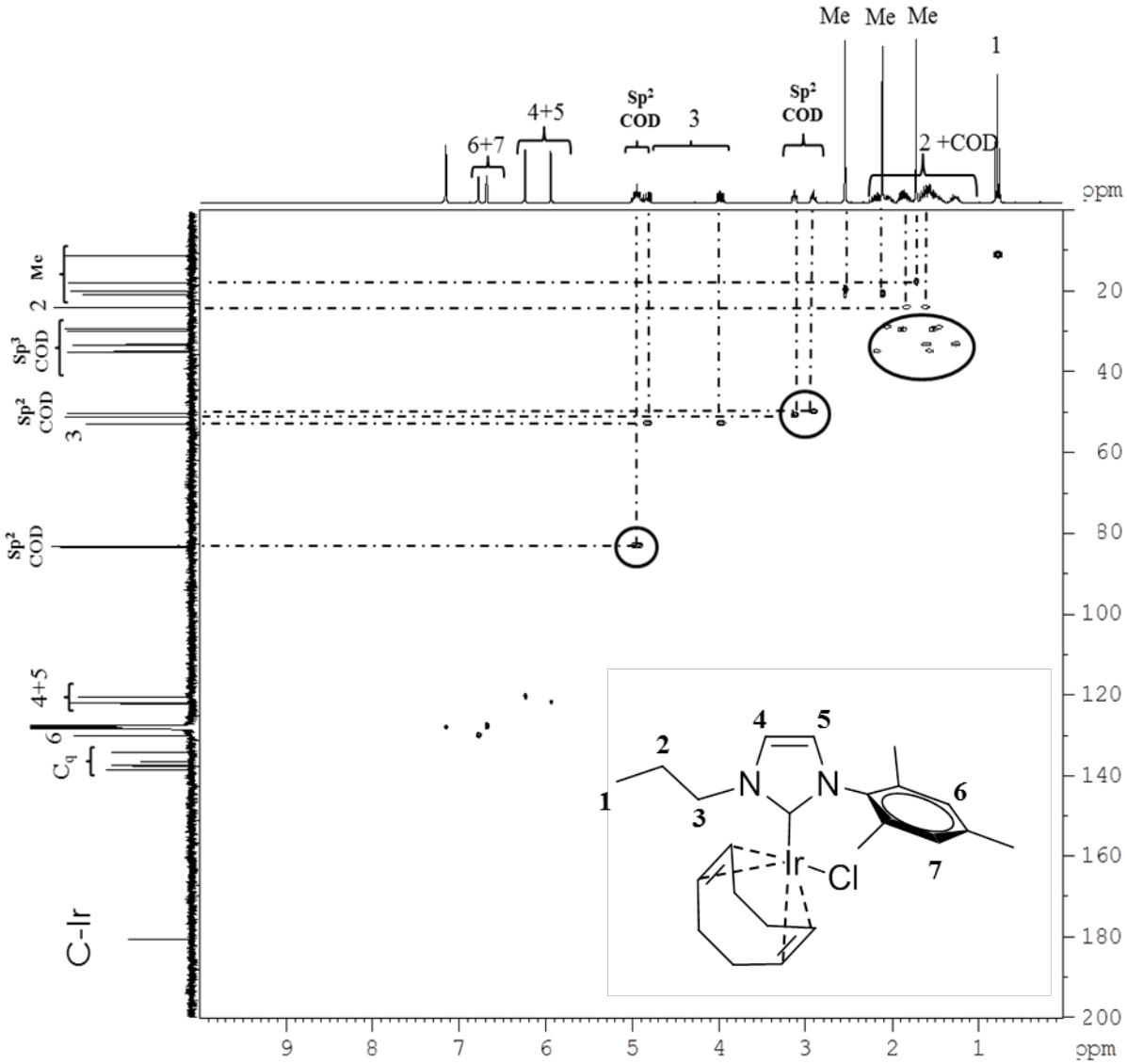

Figure S5. ^{1}H - ^{13}C HMQC NMR spectrum of **[IrCl(COD)(MesImPr)] 1** in C_6D_6. Correlations corresponding to COD are encircled.

4. X-Ray diffraction analysis of 1

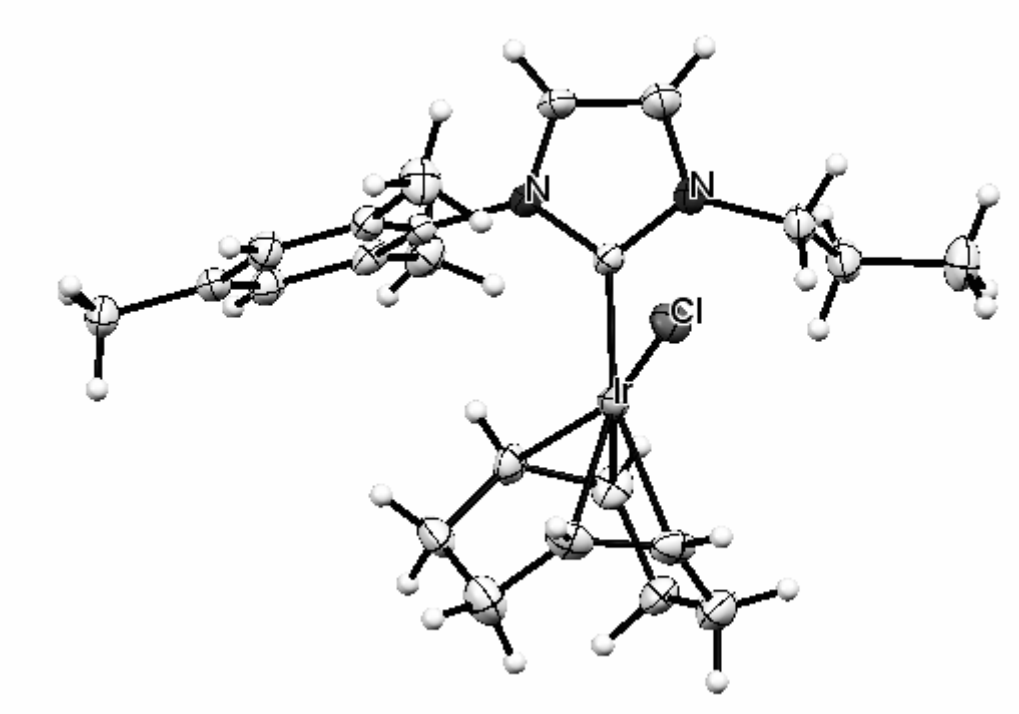

Figure S6. Crystal structure of **1** defined by X-Ray diffraction **(CCDC 1043116)**

Table S1. Crystal data structure refinement for 1.

$C_{23}H_{32}ClIrN_2$	$Z = 2$
$M_r = 564.19$	$F(000) = 556$
Triclinic, $P\bar{1}$	$D_x = 1.731$ Mg m^{-3}
Hall symbol: -P 1	Mo $K\alpha$ radiation, $\lambda = 0.7107$ Å
$a = 9.9815$ (3) Å	Cell parameters from 10034 reflections
$b = 10.2821$ (3) Å	$\theta = 3.7–29.0°$
$c = 11.5971$ (4) Å	$\mu = 6.30$ mm^{-1}
a = 97.793 (3)°	$T = 150$ K
b = 95.183 (3)°	Needle, yellow
g = 111.720 (3)°	0.82 × 0.45 × 0.30 mm
$V = 1082.66$ (7) Å^3	

Data collection

Xcalibur, Eos, Nova diffractometer	5218 independent reflections
Radiation source: Mova (Mo) X-ray Source	4820 reflections with $I > 2.0s(I)$
mirror	$R_{int} = 0.093$
Detector resolution: 15.9897 pixels mm^{-1}	$\theta_{max} = 29.2°$, $\theta_{min} = 3.1°$
w scans	$h = -12 \rightarrow 13$
Absorption correction: analytical *CrysAlis PRO*, Agilent Technologies, Version 1.171.36.28 (release 01-02-2013 CrysAlis171 .NET) (compiled Feb 1 2013,16:14:44) Analytical numeric absorption correction using a multifaceted crystal model based on expressions derived by R.C. Clark & J.S. Reid. (Clark, R. C. & Reid, J. S. (1995). Acta Cryst. A51, 887-897)	$k = -14 \rightarrow 14$
$T_{min} = 0.087$, $T_{max} = 0.292$	$l = -15 \rightarrow 15$
18778 measured reflections	

Refinement

Refinement on F^2	Primary atom site location: structure-invariant direct methods
Least-squares matrix: full	Hydrogen site location: difference Fourier map
$R[F^2 > 2\sigma(F^2)] = 0.042$	H-atom parameters constrained
$wR(F^2) = 0.104$	Method = Modified Sheldrick $w = 1/[\sigma^2(F^2) + (0.07P)^2 + 0.0P]$, where $P = (\max(F_o^2,0) + 2F_c^2)/3$
$S = 0.97$	$(\Delta/\sigma)_{max} = 0.001$
5210 reflections	$\Delta\rangle_{max} = 2.79$ e $Å^{-3}$
244 parameters	$\Delta\rangle_{min} = -3.66$ e $Å^{-3}$
0 restraints	

A Suitable crystal was selected and mounted on a Gemini kappa-geometry diffractometer (Agilent Technologies UK Ltd) equipped with an Atlas CCD detector and using Mo radiation (λ= 0.71073 Å).

Intensities were collected at 100 K by means of the CrysalisPro software. [1] Reflection indexing, unit-cell parameters refinement, Lorentz-polarization correction, peak integration and background determination were carried out with the CrysalisPro software. [2] An analytical absorption correction was applied

using the modeled faces of the crystal. [3] The resulting set of hkl was used for structure solution and refinement.

The structures were solved by direct methods with SIR97 [4] and the least-square refinement on F2 was achieved with the CRYSTALS software. [5]

All non-hydrogen atoms were refined anisotropically. The hydrogen atoms were all located in a difference map, and then were repositioned geometrically. The H atoms were initially refined with soft restraints on the bond lengths and angles to regularize their geometry (C---H in the range 0.93--0.98 Å) and Uiso(H) (in the range 1.2-1.5 times Ueq of the parent atom), after which the positions were refined with riding constraints.

4. TEM pictures of M-Ir and corresponding EDX analyses

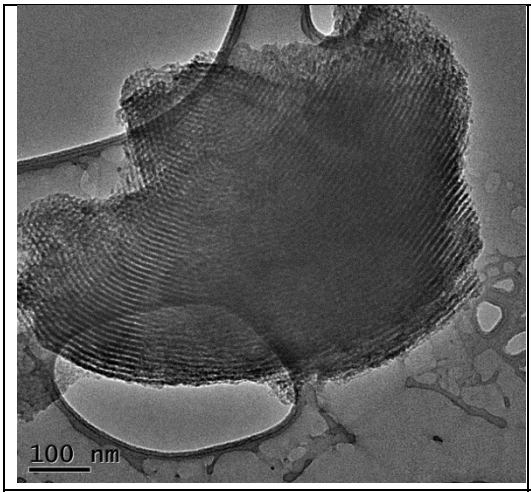

a)

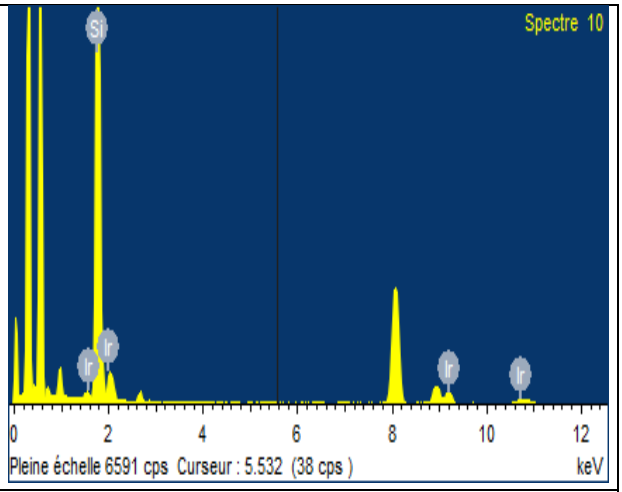

b)

c)

Element	Masse %	Atomic %
Si (K)	94.21	99.11
Ir (M)	5.79	0.89

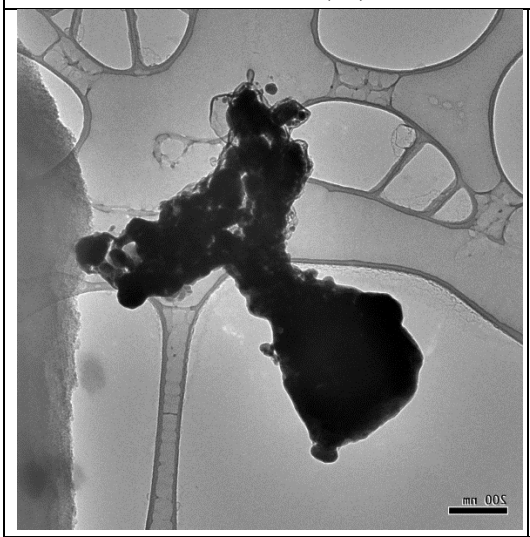

d)

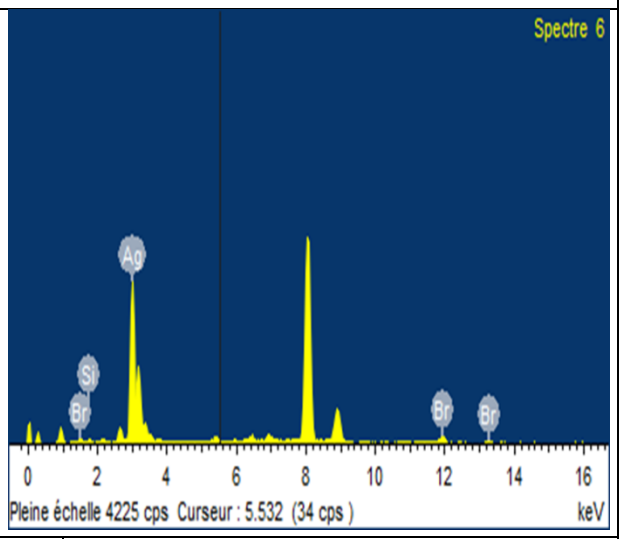

e)

f)

Element	Masse %	Atomic %
Si (K)	0.44	1.68
Br (L)	1.05	1.40
Ag (L))	98.50	96.92

Figure S7. a) and d) TEM micrographs of **M-Ir**, b) and e) EDX spectra of respective regions, c) and f) element masse and atomic percent calculated from EDX spectra.

6. Synthesis and characterization of ^{13}C labelled materials

The synthesis of the ^{13}C labelled-material was performed in the same way as for the non-labelled one by using C2-^{13}C–labelled mesitylimidazole. **M-Im***, **M*-Ag**, **M*-Ir** were prepared.

All labelled materials were characterized by conventional solid-state MAS-NMR spectroscopy. The experiments were carried out on a Bruker AVANCE III narrow bore spectrometer operating at a ^{1}H Larmor frequency of 800 MHz using a 3.2 mm probe.

TableS2. NMR parameters

Materials	All	All	M-Im*	M*-Ag/M*-Ir
Pulse Sequence	Hahn Echo	CP/MAS	HETCOR	HETCOR
Nuclei	^{1}H	^{13}C	^{1}H-^{13}C	^{1}H-^{13}C
Number of scans	8	20480	1024	1152/1984
Recycle Delay (s)	10	2.0	2.0	2.0
Spinning rate (kHz)	22	22	22	22
Acquisition length (number of points)	3244	4096	5120	5120
^{1}H 90° pulse width [π/2] (μs)	2.5	2.5	2.5	2.5
Rotor period	1	-	-	-
Contact pulse length (ms)	-	2	0.5/2	2
^{1}H rf field during contact pulse (kHz)	-	81	81	81
X rf field during contact pulse (kHz)	-	106	106	106
^{1}H magic pulse width (μs)	-	-	1	1
^{1}H rf field during eDUMBO decoupling (kHz)	-	-	100	100
Number of increments	-	-	64	74/72
Size of increments	-	-	32	64

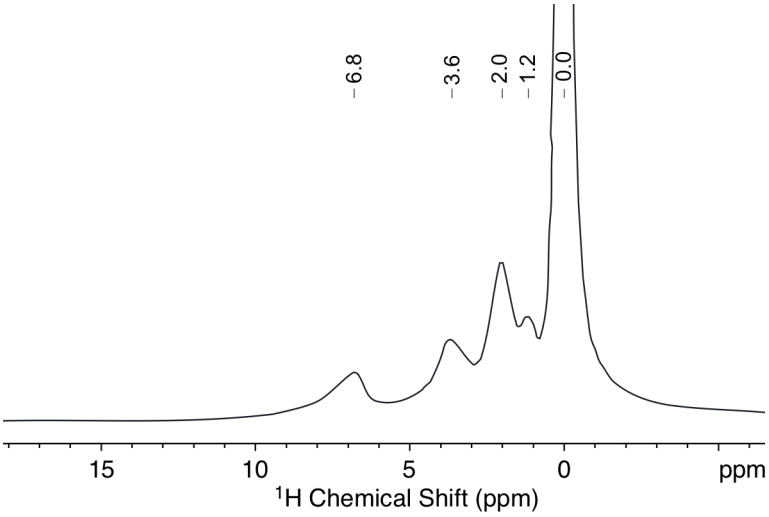

Figure S8. ^{1}H Hahn echo NMR spectrum of **M*-Ir**.

.

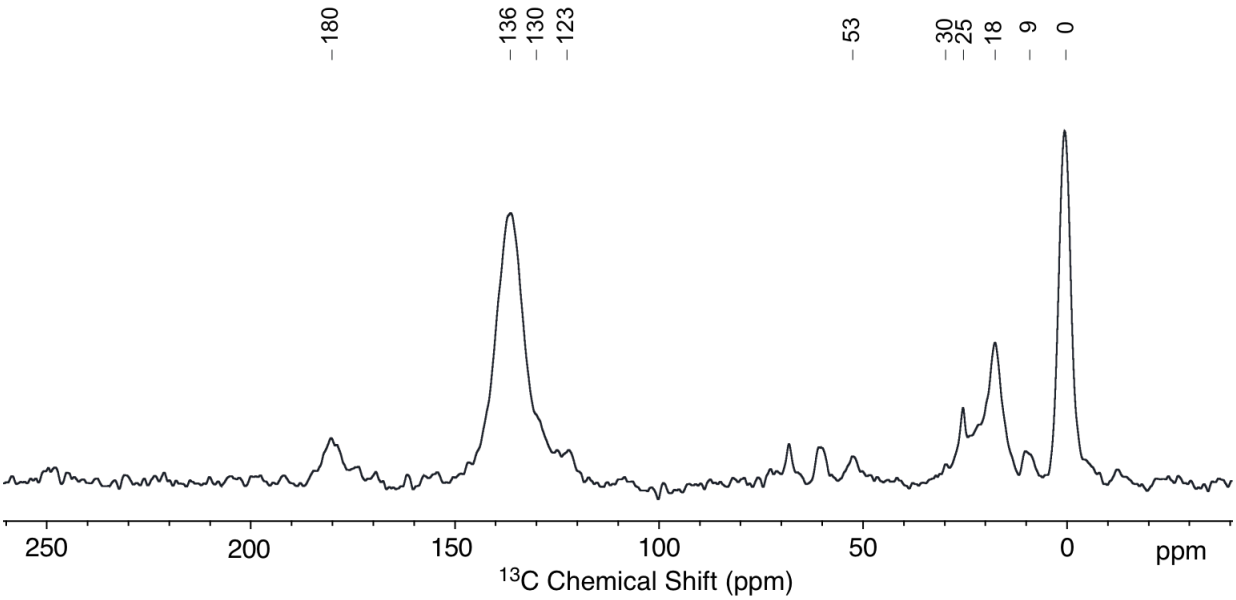

Figure S9. ^{13}C CP MAS NMR spectrum of **M*-Ir**.

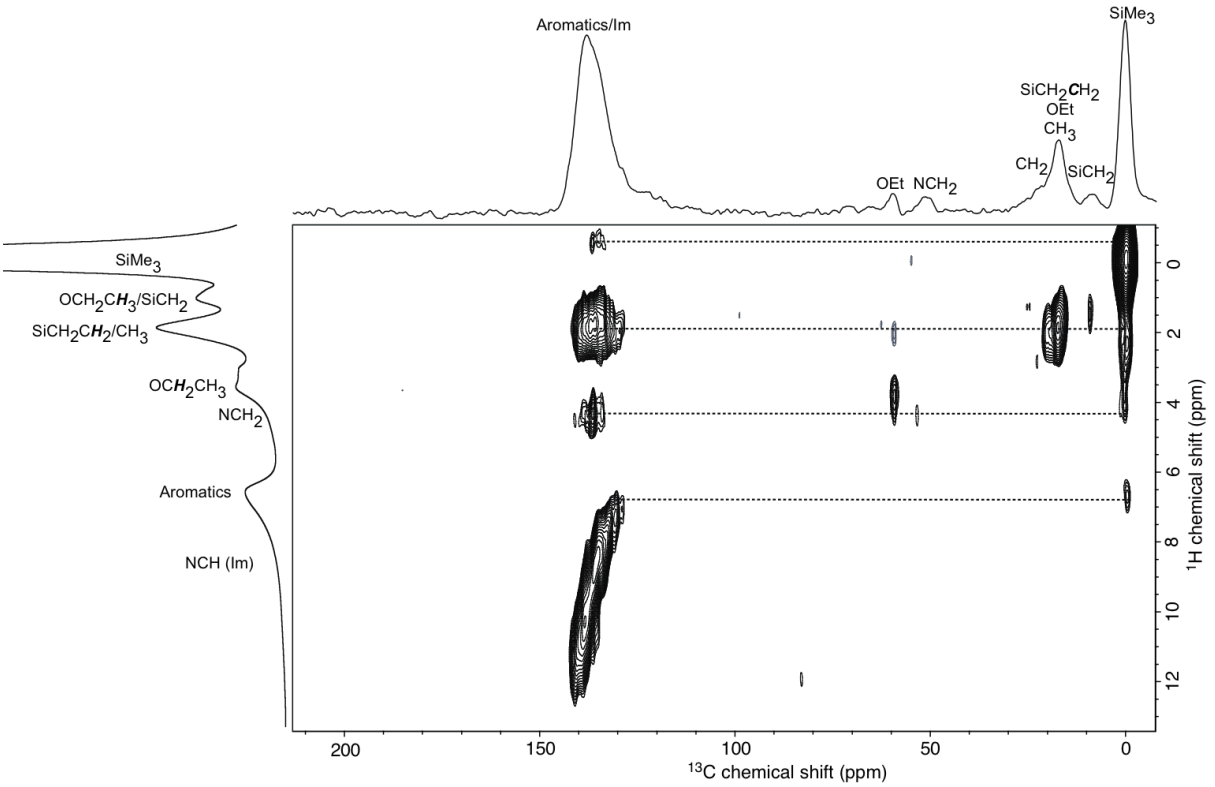

Figure S10. ^{1}H-^{13}C HETCOR NMR spectrum of **M*-Im** with long distance correlations (contact time = 2 ms). The top trace is the corresponding 1D ^{13}C CPMAS spectrum and the left trace the corresponding 1D ^{1}H Hahn echo spectrum. Crosspeaks between protons of the TMS groups (0 ppm), of the CH_3 of mesityl groups (2 ppm), and of the NCH_2 moities (4.2 ppm) with the aromatic carbons at 130 ppm are observed. Long-range correlations are shown by dashed lines.

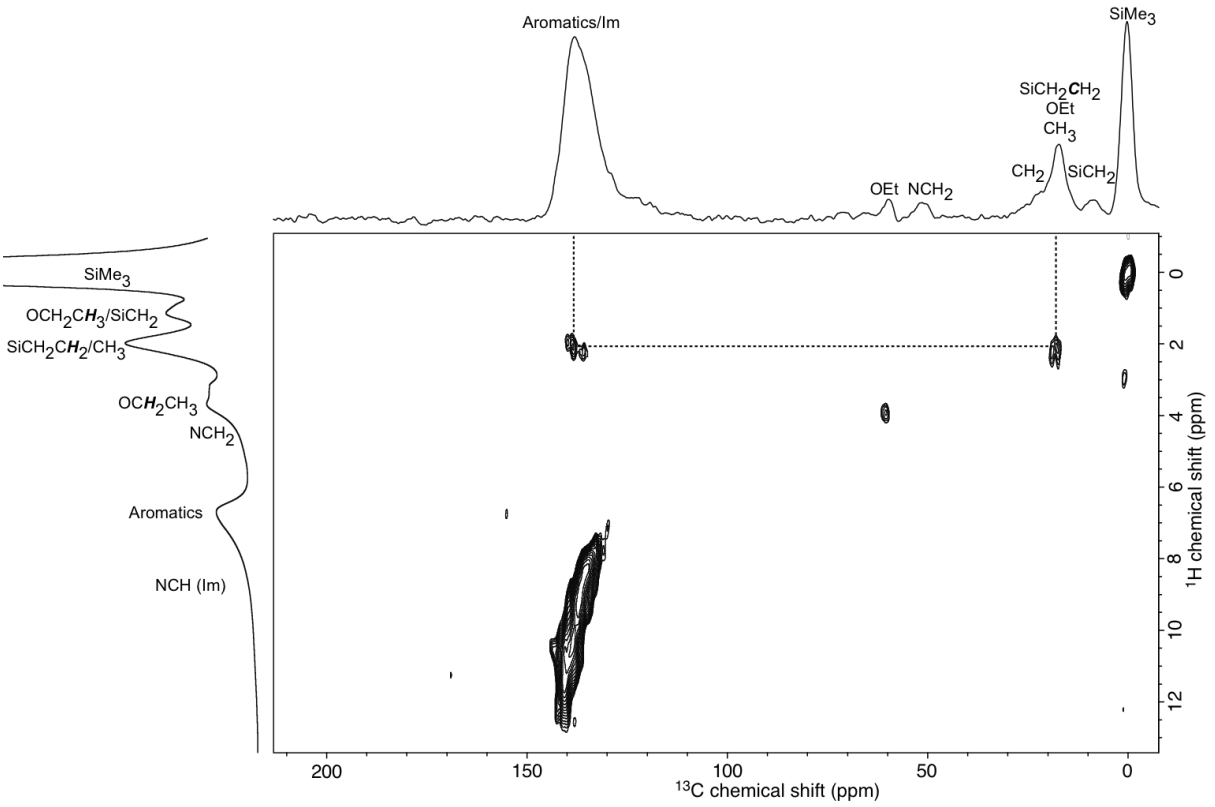

Figure S11. ^{1}H-^{13}C HETCOR NMR spectrum of M-Im* with short distance correlations (contact time = 500 μs). The top trace is the corresponding 1D ^{13}C CPMAS spectrum and the left trace the corresponding 1D ^{1}H Hahn echo spectrum. The crosspeak at 140 ppm in ^{13}C dimension and 2 ppm in ^{1}H dimension correspond to (expected) spatial proximities between methyl substituents of mesityl and the aromatic part. Dashed line underlines these spatial interactions.

7. Characterization of Iridium(I) based NHC material by DNP method

10 mg of dry powder was wetted with 20 mL of 16 mM solution of bCTbK in 1,1,2,2-tetracholorethane. The mixture was packed in 3.2mm sapphire rotor and quickly inserted in DNP spectrometer. The precise description of sample preparation can be found in our earlier articles.[2] Conditions applied for DNP measurements summarized in TableS3.

TableS3. SENS DNP NMR parameters

Pulse Sequence	CP/MAS	CP/MAS solid echo	CP/MAS	HETCOR Solid echo	HETCOR
Nuclei	^{13}C	^{13}C	^{29}Si	^{1}H-^{13}C	^{1}H-^{29}Si
MW ON/OFF	MW ON/OFF	MW ON	MW ON/OFF	MW ON	MW ON
Number of scans	64	8192	32/64	128	128
Recycle Delay (s)	2.0	2.0	2.0	1.5	2.0
Spinning rate (kHz)	8	9	8	11	11
Acquisition length (number of points)	1608	4096	4096	810	718
^{1}H 90° pulse width [π/2] (μs)	2.5	2.5	2.5	2.5	2.5
Rotor period	-	40	-	25	-
Contact pulse length (ms)	1	2	6	0.5	0.2/2
^{1}H rf field during contact pulse (kHz)	82	82	82	82	82
X rf field during contact pulse (kHz)	124	122	147	122	129
^{1}H magic pulse width (μs)	-	-	-	1	1
^{1}H rf field during eDUMBO decoupling (kHz)	-	-	-	100	100
Number of increments	-	-	-	128	128
Size of increments (μs)	-	-	-	64	64

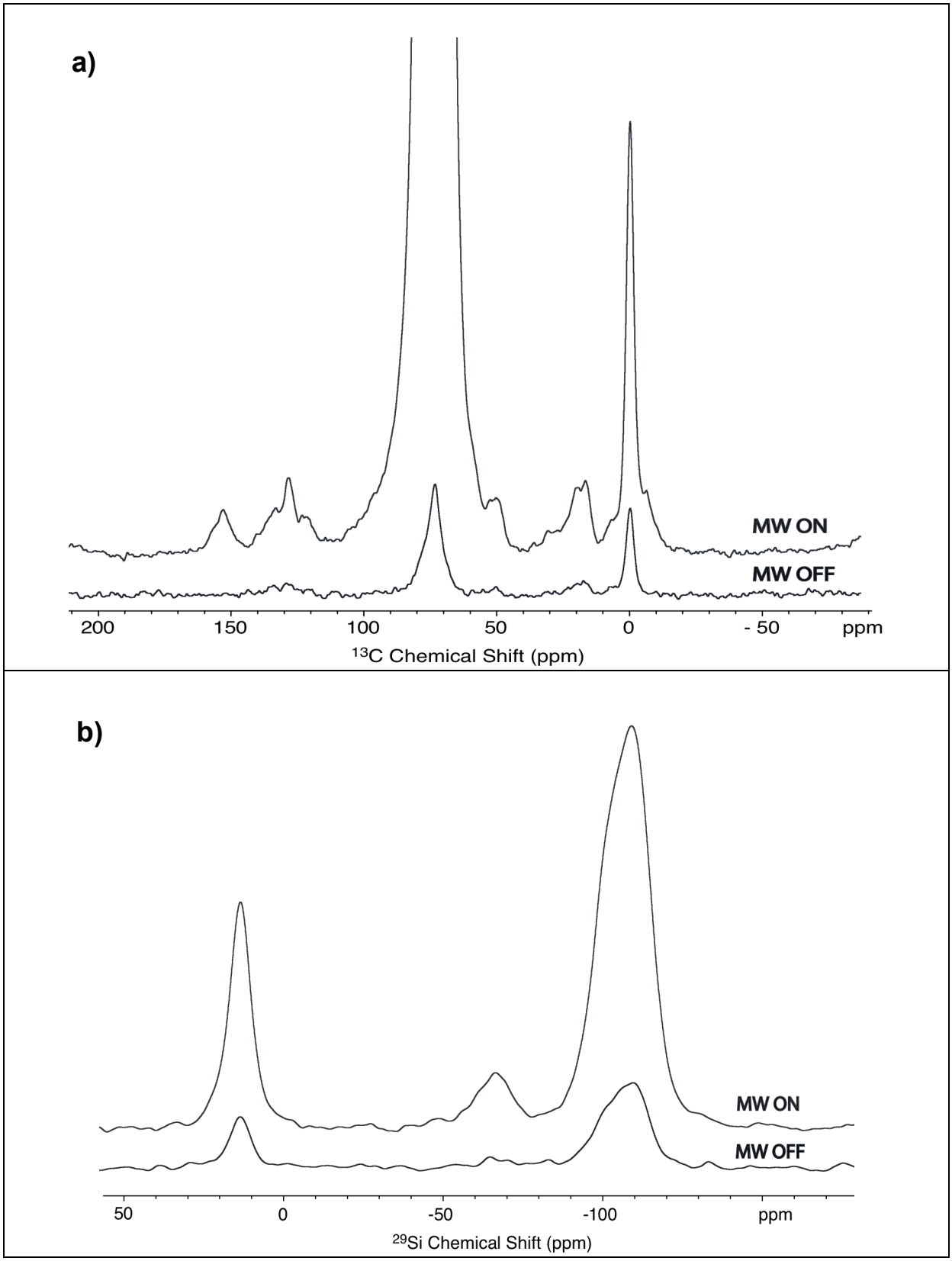

Figure S12. ^{13}C (a) and ^{29}Si (b) DNP MAS-NMR spectra of M-Ir recorded with mW irradiation on and off. The DNP enhancements were $\varepsilon = 5.1$ and $\varepsilon = 4.8$ for ^{13}C and ^{29}Si CPMAS spectra respectively.

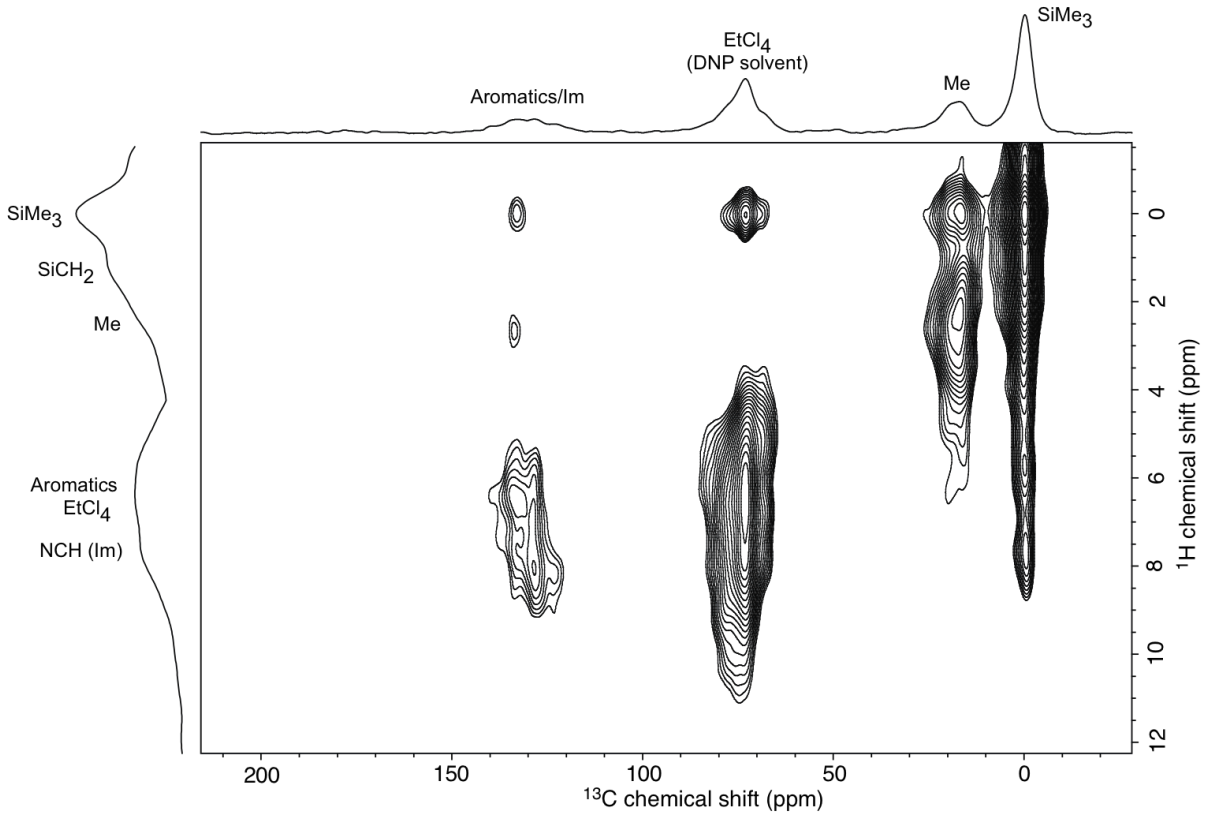

Figure S13. 2D ^{1}H-^{13}C HETCOR with solid echo (25 rotor periods) spectrum of **M-Ir** acquired with 0.5 ms contact time under DNP conditions. The top trace corresponds to the 1D ^{13}C CPMAS solid echo spectrum and the left trace to the ^{1}H internal projection (on the 1D ^{1}H spectrum, only solvent is observable). Correlations at 50 ppm in ^{13}C dimension and 3 ppm in ^{1}H dimension as well as correlations at 25-35 ppm in ^{13}C dimension and 5 ppm in ^{1}H dimension corresponding to the sp^2 and sp^3 hybridized carbons of COD respectively could not detected. However the correlation between aromatic carbons at 140 ppm in ^{13}C dimension and 0 ppm in the ^{1}H dimension (TMS protons) as well as correlations at 0 ppm in ^{13}C dimension with 7-10 ppm in ^{1}H dimension suggest the folding of organic functionalities onto the surface, as observed already with conventional solid-state NMR spectroscopy.

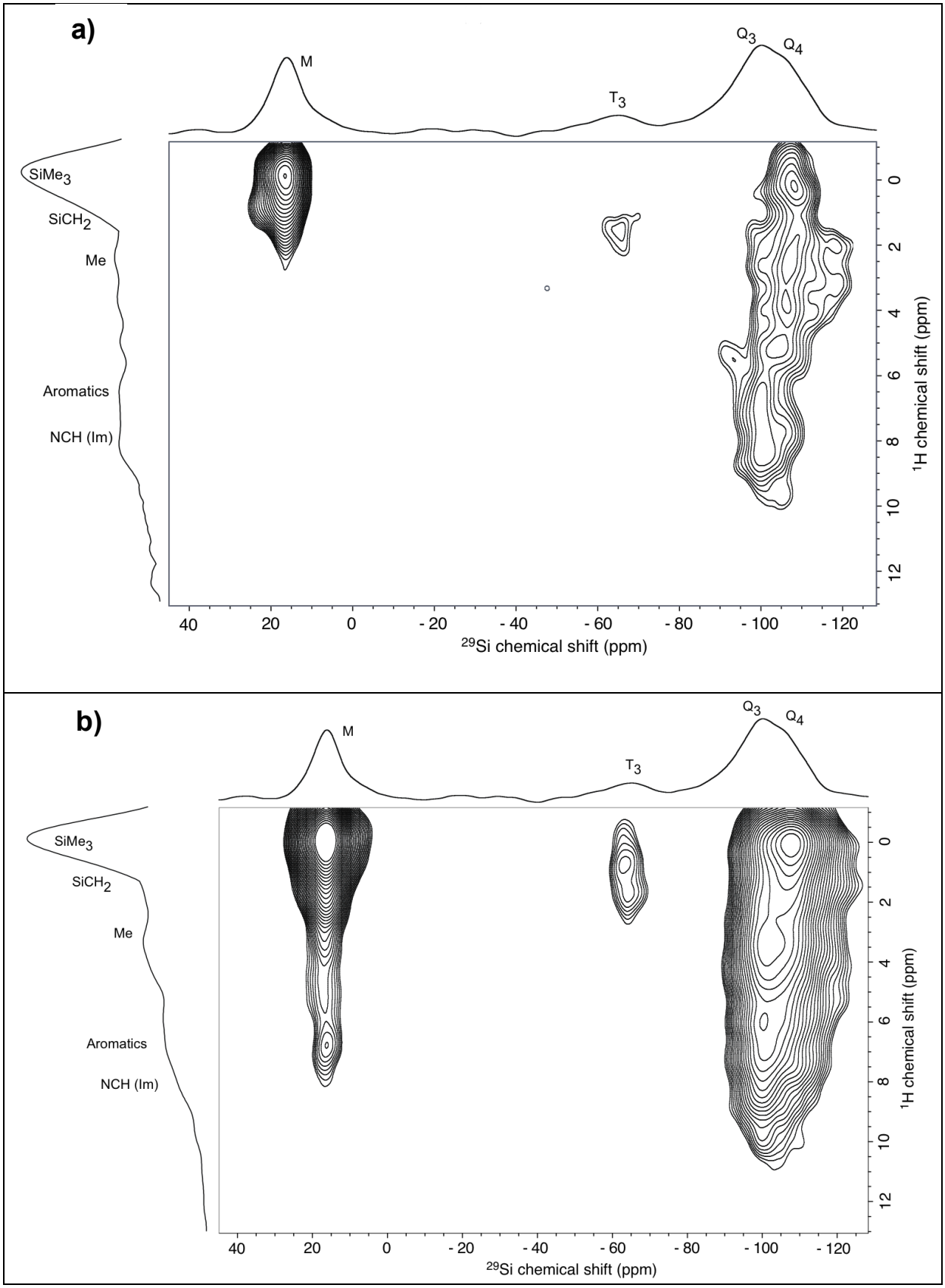

Figure S14. 2D ^{1}H-^{29}Si HETCOR spectra of **M-Ir** acquired with short (0.2 ms, **a**) and long (2.0 ms, **b**) contact times under DNP conditions. The top traces correspond to the 1D ^{29}Si CPMAS solid echo spectrum and the left traces to the

^{1}H internal projection (on the 1D ^{1}H spectrum, only solvent is observable). Crosspeaks at 20 ppm in ^{29}Si dimension and 2-7 ppm in ^{1}H dimension are assigned to spatial proximities between the TMS groups and the organic functionalities ($2CH_3$ of mesityl at 2 ppm, NCH_2 at 4 ppm, aromatic protons at 7 ppm), illustrating again the folding of the organic functionalities onto the surface.

8. NMR experiments under H_2 pressure for COD concentration determination

The detection of cyclooctane release from material was performed in high pressure stable (up to 7 bars) QVP NMR tube. The NMR tube is prepared under inert atmosphere, with 36 mg of material **M-Ir** (0.006 mmol of Ir), 2.8 ml of dry degased C_6D_6 and 10 µL (0.094 mmol) of dry degased toluene as a standard. The tube was then pressurized under 3 bars of H_2 and the reaction was monitored by ^{1}H NMR at 25 °C. The appearance of a signal at 1.5 ppm corresponding to cyclooctane product was detected (Figure S16). No more release of cyclooctane was detected after 27 h reaction. To confirm the cyclooctane formation 0.5 µL of pure cyclooctane was added to the NMR tube (Figure S16).

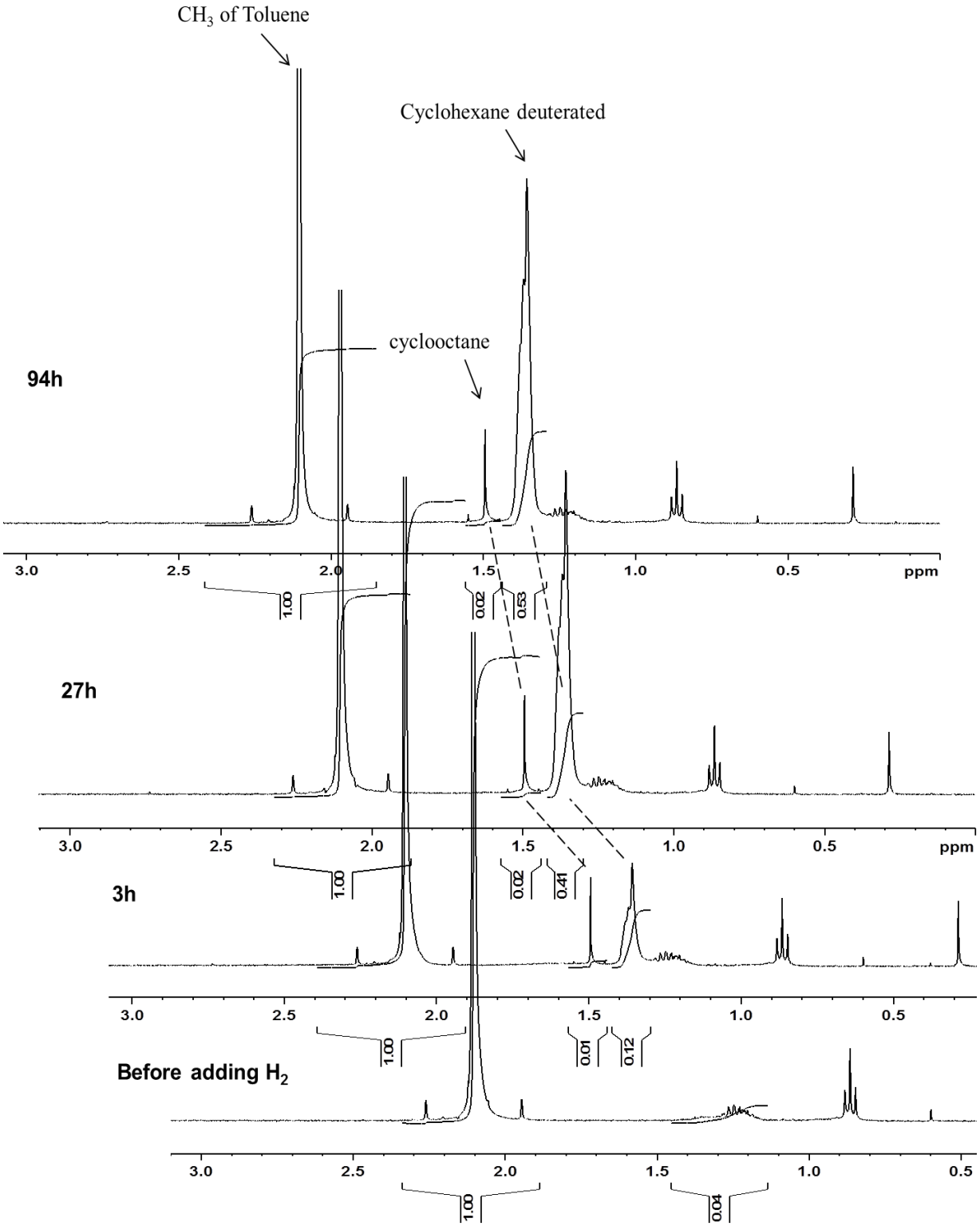

Figure S15. *In situ* ^{1}H NMR detection of cyclooctane (C_6D_6, 300K; 400MHz)

Beside the evolution of cyclooctane (1,5 ppm), the hydrogenation of C_6D_6 is observed, as shown by the growth of a broad signal at ca. 1.37 ppm, corresponding to deuterated cyclohexane. This result is suggests the formation of Ir NPs during the experiment thus showing that such NPS are only formed

when no olefinic substrate is present. This result is further confirmed by TEM micrographs and EDX performed on the recovered material after 94h under H_2 in C_6D_6 (See fig. S17).

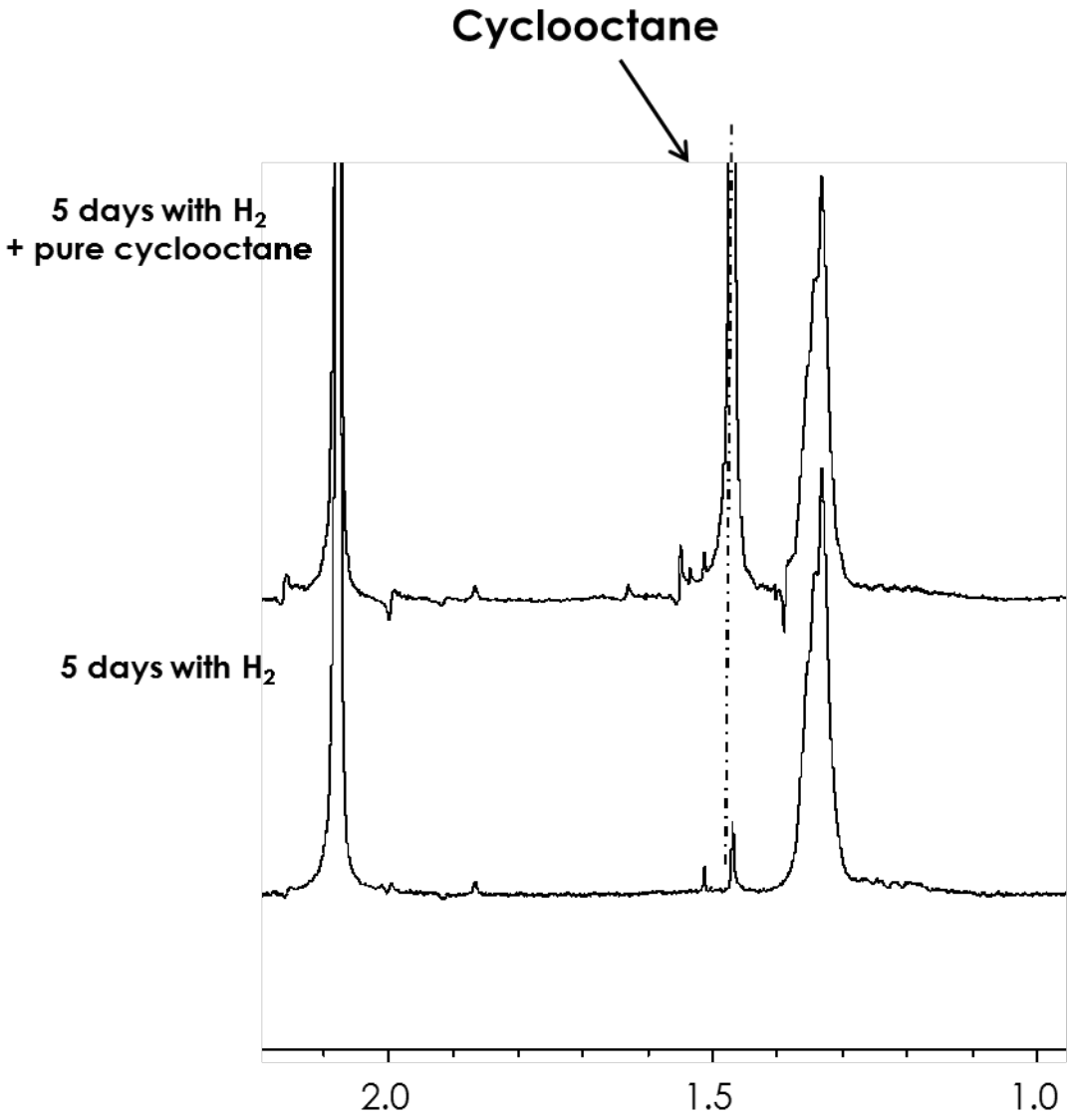

Figure S16. ^{1}H NMR detection of cyclooctane (C_6D_6, 300K; 300MHz)

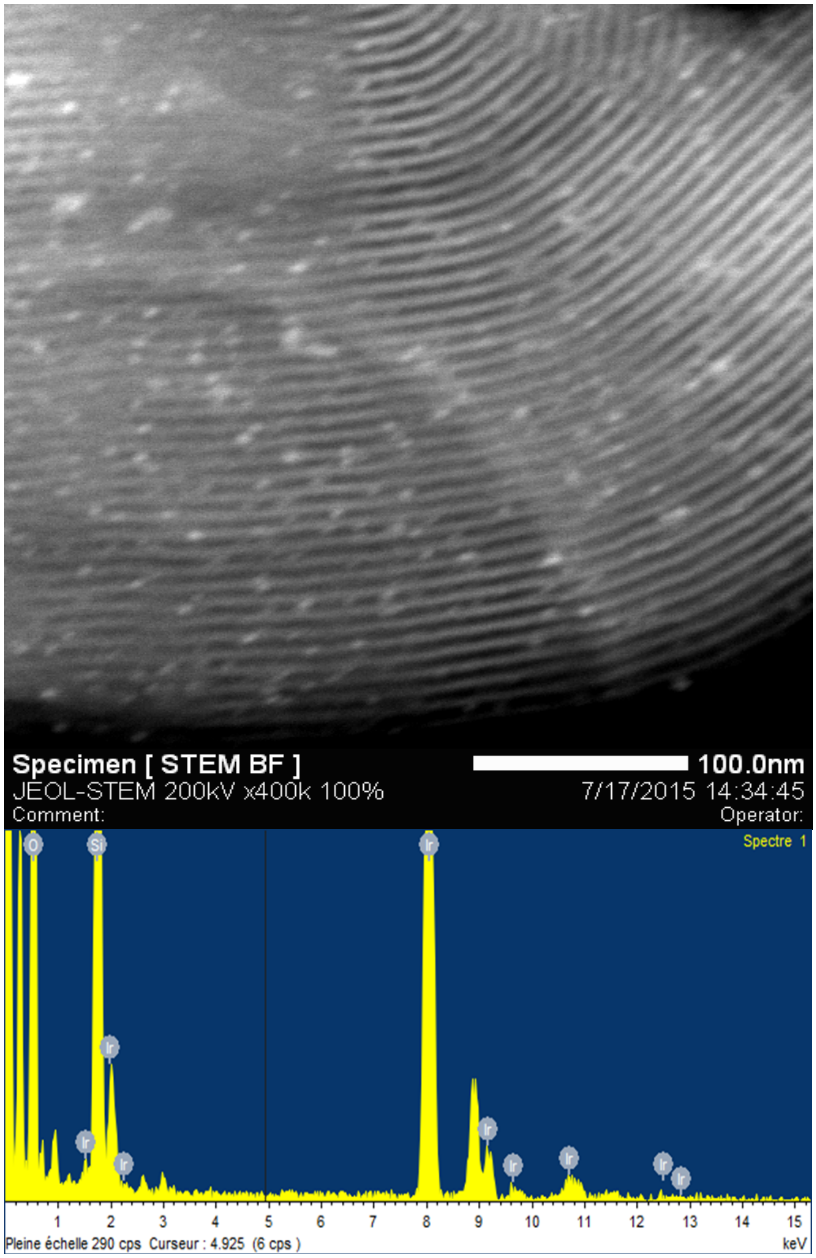

Figure S17. STEM micrograph and EDX of the recovered solid after 94 hours under H_2 in C_6D_6 and toluene as internal standard.

9. Procedures for catalytic experiments with homogeneous [IrCl(COD)(MesImPr)], [Ir(COD)(MesImPr)]BF_4 and heterogeneous Iridium(I) based NHC material

All the tests were performed in specifically adapted glass reactor with connection to vacuum, argon and hydrogen lines. The catalyst, substrates and internal standard were introduced into the reactor under argon using standard Schlenk techniques. Trans-stilbene was received from Sigma-Aldrich and was recrystallized from methanol prior to use. Before each catalytic test, reactor was purged with Argon. The catalysis performed with 0.1 mol% of catalyst (corresponding to Ir) at 40 °C under 3 bars of H_2 pressure. Reaction was monitored by ^{1}H NMR. The conversion was measured by relative disappearance of peak at 3.78 ppm which corresponds to =CH of double bond and appearance of peak at 2.98 ppm which corresponds to -CH_2 of hydrogenated product. 1, 2-tetrachloroethane was used as internal standard.

Heterogeneous catalysis

10 mg of **M-Ir** (0.0017 mmol of Ir) were mixed in a glove box with 300 mg of trans-stilbene (1.67 mmol). The mixture was dissolved in 3.5 ml of dry degassed toluene. 0.1ml of internal standard was added and all mixture was transferred to glass reactor (reactor volume=30 mL) with the help of cannula.

For the determination of maximum TON was used more diluted system (0.01mol% of catalyst). 60mg of M-Ir (0.005 mmol of Ir, batch with 25% silver to iridium conversion) were mixed in glove box with 8.460g of trans-stilbene (47 mmol). The mixture was dissolved in 85mL of dry degased toluene. 0.5ml of internal standard was added and all mixture was transferred to glass reactor (reactor volume=400mL) with the help of cannula.

Homogeneous catalysis

752 μL of 0.022 M solution of [IrCl(COD)(MesImPr)] (0.017 mmol) was introduced in a Schlenk already containing 3 g of trans-stilbene (16.7 mmol) dissolved in 35 mL of dry degassed toluene. After 0.2 ml of internal standard were added. The mixture was transferred to glass reactor (reactor volume=300ml) with the help of cannula.

The cationic species [Ir(COD)(MesImPr)]BF_4 was generated *in situ* with addition of 0.0017 mmol of $AgBF_4$ (300 μL of dry degased 0.056 M solution in

toluene) inside the glass reactor (reactor volume=300ml) before pressurizing with H_2. It was seen the precipitation of white solid of AgI.

Scope of substrates

Styrene and its derivatives with electron donating (4-vinilanisole, 4-acetoxystyrene) and election withdrawing (4-fluorostyrene) substituents were chosen as substrates for hydrogenation. The substituted styrenes were received from Sigma-Aldrich and dried with 5 Å molecular sieves prior to use. Tran-stilbene was used as a bench mark and was purified as previously described. The catalysis performed in toluene with 0.03 mol% of catalyst loading (corresponding to Ir) at 40 °C under 3 bars of H_2.

10 mg of M-Ir (0.0017 mmol) were suspended at 10ml of dry degased toluene. Solution was transferred in the reactor under Argon. 5.1mmol of Substrate was then introduced followed by addition of 0.1 mL of the internal standard.

Homogeneous and heterogeneous catalytic experiments were performed with similar conditions [IrCl(COD)(MesImPr)] was introduced as 1.4 mL of 0.001M stock solution and 8.5 mL of solvent was added.

Reactions were monitored by ^{1}H NMR. The results are presented in Figure S18 and in Table S4.

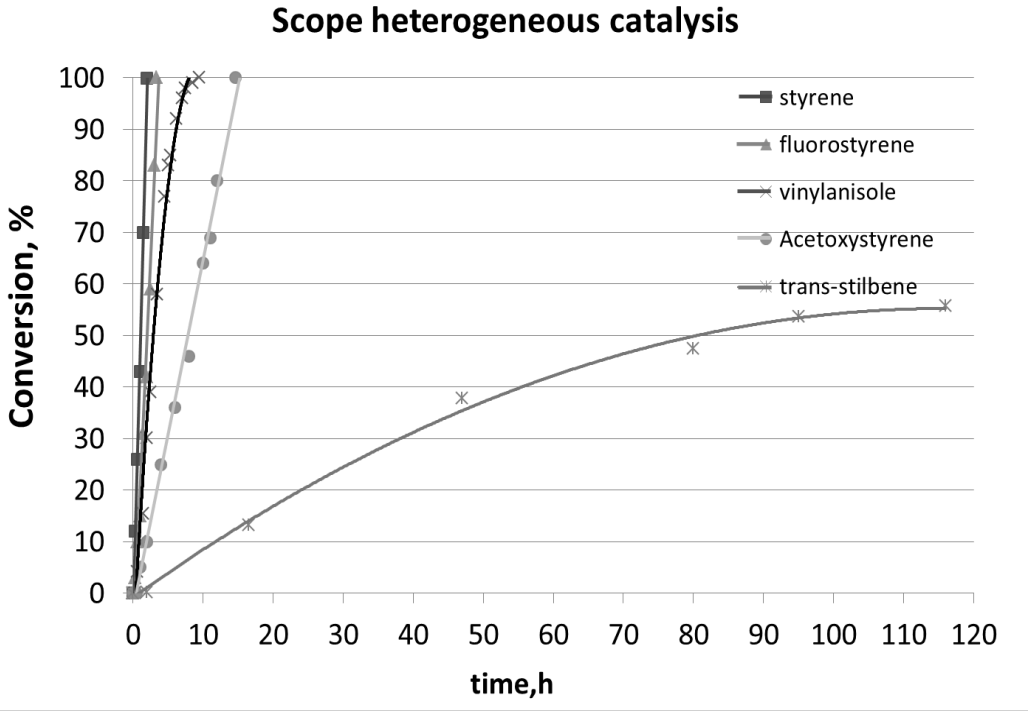

Figure S18. Scope of substrates for **M-Ir.** Conversion of alkene (%).

TableS4. Comparison of TOF (h^{-1}) for homogeneous and heterogeneous catalysts

Substrate	TOF, h^{-1}		Improvement
	M-Ir	[IrCl(COD)(MesImPr)]	
styrene	1400	177	8 times faster
4-fluorostyrene	750	170	4.5 times faster
4-vinilanisole	190	120	4 times faster
4-acetoxystyrene	490	125	1.5 times faster
t*rans*-stilbene	44	4	10 times faster
limonene	125	20	6 times

For Styrene's derivatives, the TOF (h^{-1}) was calculated at 50 % conversion. For trans-stilbene, the TOF (h^{-1}) was calculated at 50 h of reaction.

Split tests

Leaching of active species:

After full conversion of substrate (acetoxystyrene), the supernatant was collected and filtered under Ar and portion of substrate (limonene) was added. No conversion of limonene was detected during 30h (Fig. 19).

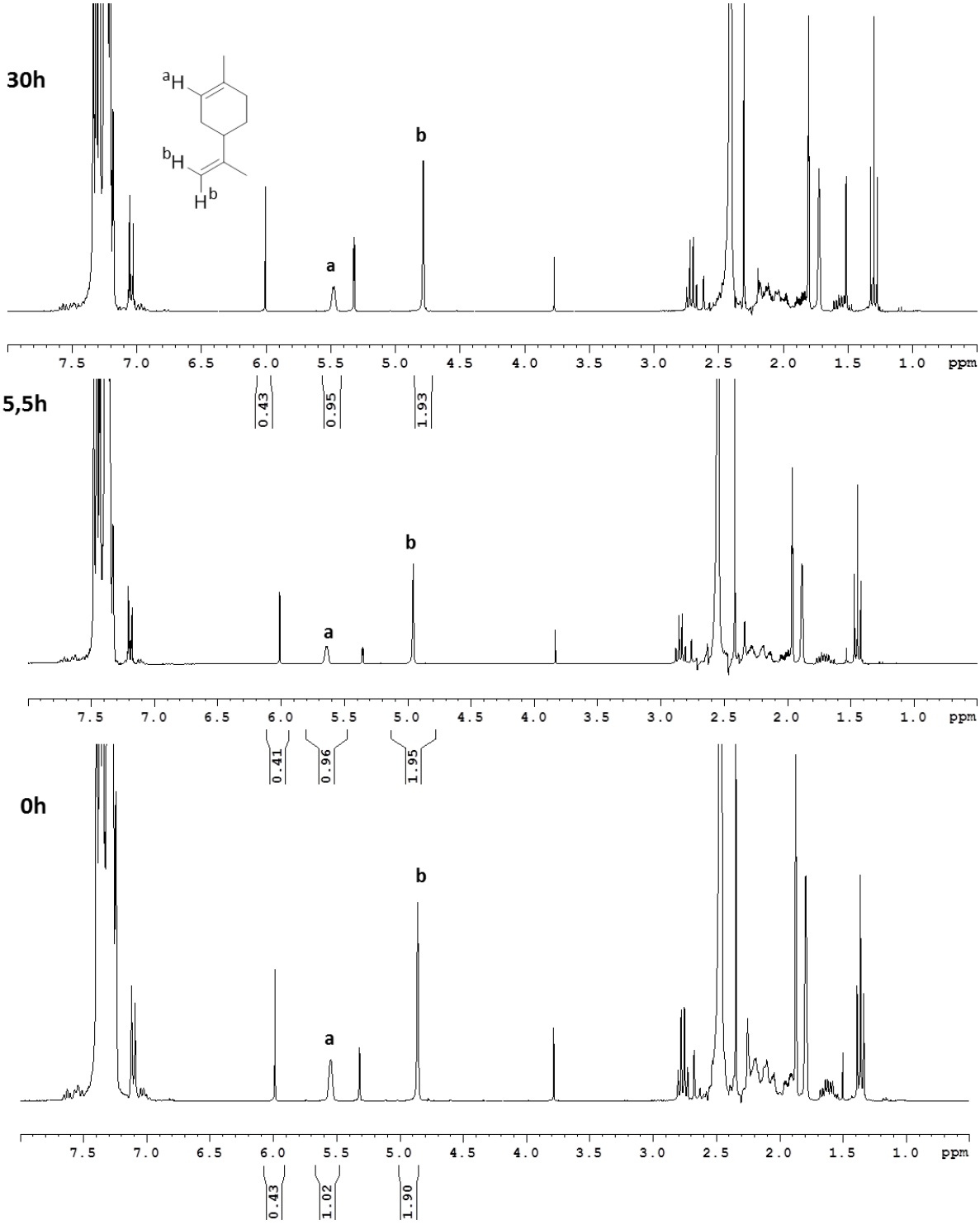

Figure S19. ^{1}H NMR spectra of limonene hydrogenation by recovered supernatant from acetoxystyrene hydrogenation

Leaching of inactive species:

After full conversion of substrate, the supernatant was collected and separate from **M-Ir** by filtration and send to elemental analysis.. According to the results, the detected Ir leaching is less than 1ppm.

References

[1] T. K. Maishal, J. Alauzun, J.-M. Basset, C. Copéret, R. J. P. Corriu, E. Jeanneau, A. Mehdi, C. Reyé, L. Veyre, C. Thieuleux*, Angew. Chem. Int. Ed*. **2008**, 47, 8654-8656.

[2] CrysAlisPro, Agilent Technologies, Version 1.171.34.49 (release 20-01-2011 CrysAlis171 .NET) (compiled Jan 20 2011,15:58:25)

[3] R. C. Clark & J. S. Reid, *Acta Cryst. A* **1995**, 51, 887-897.

[4] A. Altomare, M.C. Burla, M. Camalli, G.L. Cascarano, C. Giacovazzo, A. Guagliardi, A. Grazia, G. Moliterni, G. Polidori, R. Spagna, *J. App. Cryst.* **1999**, 32, 115-119.

[5] P.W. Betteridge, J.R. Carruthers, R.I. Cooper, K. Prout, D.J. Watkin, *J. Appl. Cryst.* **2003**, 36, 1487-1487.

[6] M. P. Conley, R.M. Drost, M. Baffert, D.Gajan, C.Elsevier, W. T. Franks, H. Oschkinat, L.Veyre, A. Zagdoun, A. Rossini, M. Lelli, A. Lesage, G. Casano, O. Ouari, P. Tordo, L. Emsley, C. Coperet, and C. Thieuleux. *Chem. Eur. J*. **2013**, 19, 12234-12238.